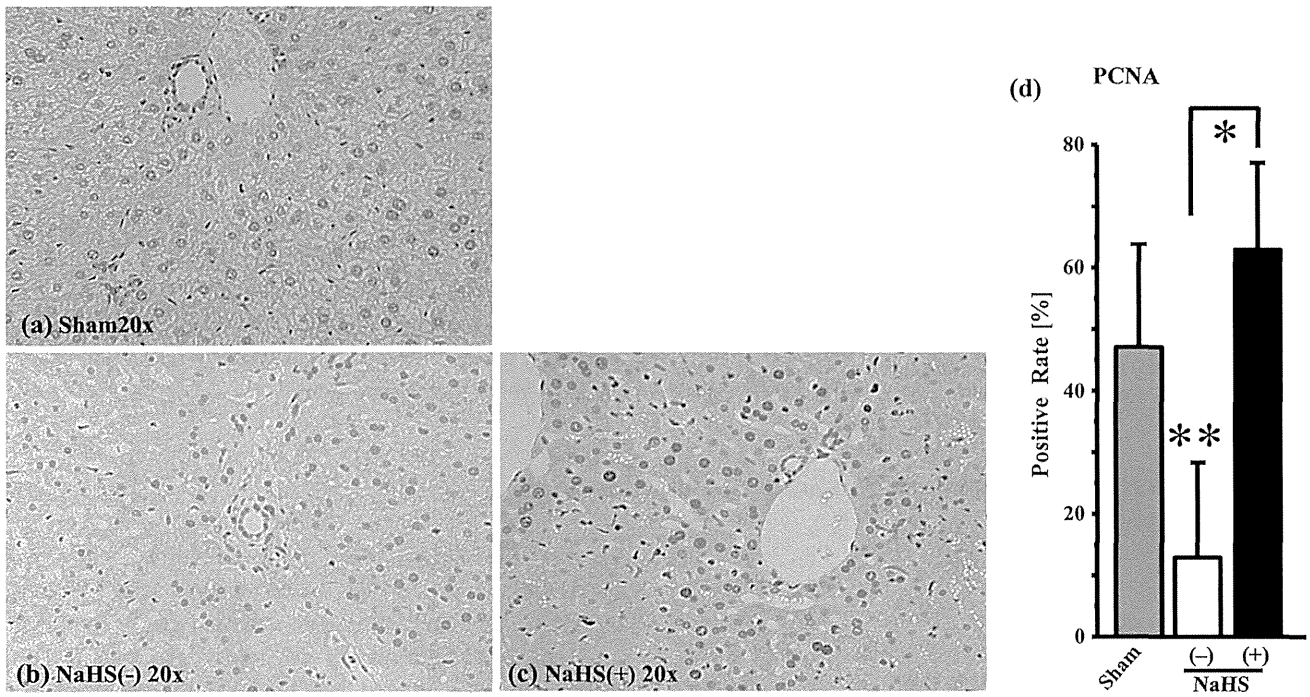

Fig. 6 Sodium hydrogen sulfide (NaHS) stimulates liver regeneration. Mice were subjected to partial warm ischemia for 75 min and subsequent reperfusion (I/R) for 24 h. Liver sections were stained by the anti-proliferating cell nuclear antigen (PCNA) antibody and hematoxylin as nuclear counterstaining. Representative photographs (20× magnification) are shown. In the sham group (**a**), the positive rate was 47 %, but it was significantly decreased in the NaHS(−) group (**b**), and it was significantly augmented in the NaHS(+) group (**c**). The rate of PCNA-positive hepatocytes is shown in (**d**). Values are expressed as the mean ± SD. $*P < 0.05$, NaHS (−) vs. NaHS (+). $**P < 0.05$ vs. Sham

In this study, serum TNF-α, IL-6, IL-1β, IFN-γ, IL-17, IL-23, and soluble CD40L (CD154) increased significantly within 3 h of reperfusion, but these changes were inhibited by NaHS. Hydrogen sulfide reduced hepatic IRI with less production of TNFα and IL-6 [16]. Suppression of the IL23–IL17 axis reduced hepatic IRI [29]. Altogether, these facts suggest that NaHS reduced hepatic IRI by inhibiting the IL23–IL17 axis, thereby inhibiting the activation of Kupffer cells, neutrophils, and lymphocytes (CD4 +/Th17 cells) in the early phase of reperfusion. Although there are various sources of CD40L, the main source is the activated platelets [30], and CD40L was found to worsen hepatic IRI [28]. In this study, there was a massive release of cytokines and chemokines at R3 h. Multiple pro-inflammatory mediators from various cell types, platelet-endothelial adhesion, and platelet-leukocyte aggregation would stimulate the further activation of platelets [2], leading to the sustained high level of soluble CD40L.

Oxidative stress is another important factor in hepatic IRI [2–4]. Oxidative damage in the sinusoidal endothelial cells stimulates endothelin-1 (ET-1) production, leading to microcirculatory disturbance [31, 32]. Several distinct mechanisms of the anti-oxidant property of H_2S have been reported, namely, direct scavenging of ROS [33], reversible inhibition of mitochondrial respiration [34], augmentation of glutathione (GSH) production through enhanced cystine/cysteine transport [35], and Nrf2-dependent expression of anti-oxidant and anti-inflammatory proteins [23]. Consistent with these reports, NaHS reduced lipid peroxidation and inflammation in this study.

Nrf2 exists in the cytosol with Keap-1 in the resting state, but it dissociates from Keap-1 on exposure to stimuli, such as oxidative stress and pro-survival signals, leading to up-regulation of HO-1 [36] and TRX-1 [37]. HO-1 reduces oxidative stress through the conversion of heme into biliverdin and carbon monoxide (CO) [38]. Furthermore, CO exerts anti-inflammatory and vasodilatory effects [39] and TRX-1 reduces protein thiol and/or hydrogen peroxide with the support of GSH [40]. In line with these reports, our study showed, for what we believe to be the first time, that NaHS augmented HO-1 and TRX-1 levels through augmented nuclear translocation of Nrf2, leading to reductions in oxidative stress and inflammation.

The anti-apoptotic and pro-survival effects of H_2S against mitochondria would result in an inhibition of intrinsic apoptosis [36]. H_2S activates this pathway in the I/R of hippocampal neurons [7, 41] and myocardium [5]. Insulin supplementation has been shown to stimulate

myocardial surviving expression via activation of PI3K-Akt-mTOR-p70s6k, resulting in anti-apoptotic effects [42]. In this study, pro-survival signals mediated by the PDK-1-Akt-mTOR-p70s6k axis were maintained by the higher phosphorylation in the NaHS-treated liver. Phosphorylation of p70s6k confers protection against IRI in the heart and small intestines through anti-apoptotic and anti-inflammatory effects [17, 18]. The enhanced PDK1-Akt signal reduced IRI through the augmented phosphorylation of PDK1 [43] and Akt [14], but not through de novo gene expression of these proteins, at least within 6 h of reperfusion. In line with these reports, this study is the first to show that NaHS supplementation ameliorated hepatic warm IRI by maintaining the phosphorylation of p70s6k and upstream kinases, including mTOR, Akt, and PDK-1. Since we did not assess any gene expression, further study is required to clarify the precise mechanism of NaHS-mediated protection during the early phase of reperfusion.

Another important anti-apoptotic signal in hepatic IRI is the signal transducer and activator of transcription 3 (STAT3) [9]. Ke et al. [29] recently reported that HO-1 ameliorated hepatic inflammation, apoptosis, and net injury after warm I/R by inhibiting NF-kappaB signals in the nucleus. They showed that STAT3 was indispensable for the HO-1-mediated down-regulation of TLR-4 and PTEN, and the augmentation of phospho-Akt. In the present study we observed a transient rise of IL-6 at 3 h, only slight increases of IL-6 and TNF-α at 6 h, and a significantly higher PCNA-positivity rate 24 h after reperfusion in the NaHS-treated group. Debonera et al. [44] reported that IL-6-mediated activation of STAT3 did not trigger liver regeneration in severely injured liver grafts. Although we did not evaluate STAT3 here, these observations suggest that the STAT3-mediated machinery of liver regeneration [45] would have functioned well in the NaHS-treated liver.

Recently, Zhang et al. [46] reported that NaHS administration before ischemia inhibited mitochondrial permeability transition pore opening and activated Akt-GSK3β. Exogenously administered hydrogen sulfide disappeared rapidly from the blood and tissues through oxidation and thiol-binding [47], with half-lives of 2.0 and 5.4 min in the aerobic and anaerobic liver, respectively [48]. Therefore, we administered NaHS before reperfusion to maintain enough concentration at reperfusion. In contrast to the previous report [46], we failed to show the efficacy by administration before ischemia in our preliminary study. In relation to dosage, Kang et al. [15] reported the effective dose to be 0.78 mg/kg. Since 0.5 mg/kg was less effective than 1 mg/kg, and 3 mg/kg resulted in animal death by respiratory dysfunction in our preliminary study, we adopted 1 mg/kg as the optimal dose (data not shown). The controversy might be due to the differences in ischemia time, species, and strain. Although further investigation is necessary to establish the optimal mode of administration for liver graft protection, it is encouraging that hydrogen sulfide proved effective when administered before ischemia [46], before reperfusion, and during cold preservation [49].

In conclusion, NaHS treatment against hepatic warm I/R resulted in high phosphorylation levels of PDK1, Akt, mTOR, and p70S6k, and nuclear translocation of Nrf2, leading to anti-oxidant, anti-inflammatory, anti-apoptotic, pro-survival, and pro-proliferative effects, and eventually reduced net IRI with rapid liver regeneration.

Acknowledgments We thank Mr. Masatoshi Horigome and Ms. Sayaka Miyoshi for their excellent technical support. This work was supported in part by a Public Trust Surgery Fund (2012) and a grant-in aid for Scientific Research from the Ministry of Education, Science, Sports, and Culture of Japan (No. 25293272).

Conflict of interest Shingo Shimada and his co-authors have no conflicts of interest.

References

1. Monbaliu D, Pirenne J, Talbot D. Liver transplantation using donation after cardiac death donors. J Hepatol. 2012;56:474–85.
2. Vollmar B, Menger MD. The hepatic microcirculation: mechanistic contributions and therapeutic targets in liver injury and repair. Physiol Rev. 2009;89:1269–339.
3. Zwacka RM, Zhou W, Zhang Y, Darby CJ, Dudus L, Halldorson J, et al. Redox gene therapy for ischemia/reperfusion injury of the liver reduces AP1 and NF-kappaB activation. Nat Med. 1998;4:698–704.
4. Abu-Amara M, Yang SY, Tapuria N, Fuller B, Davidson B, Seifalian A. Liver ischemia/reperfusion injury: processes in inflammatory networks—a review. Liver Transpl. 2010;16:1016–32.
5. Hu Y, Chen X, Pan TT, Neo KL, Lee SW, Khin ES, et al. Cardioprotection induced by hydrogen sulfide preconditioning involves activation of ERK and PI3 K/Akt pathways. Pflugers Arch. 2008;455:607–16.
6. Tsang A, Hausenloy DJ, Mocanu MM, Yellon DM. Postconditioning: a form of "modified reperfusion" protects the myocardium by activating the phosphatidylinositol 3-kinase-Akt pathway. Circ Res. 2004;95:230–2.
7. Noshita N, Lewen A, Sugawara T, Chan PH. Evidence of phosphorylation of Akt and neuronal survival after transient focal cerebral ischemia in mice. J Cereb Blood Flow Metab. 2001;21:1442–50.
8. King AL, Lefer DJ. Cytoprotective actions of hydrogen sulfide in ischaemia-reperfusion injury. Exp Physiol. 2011;96(9):840–6.
9. Calvert JW, Jha S, Gundewar S, Elrod JW, Ramachandran A, Pattillo CB, et al. Hydrogen sulfide mediates cardioprotection through Nrf2 signaling. Circ Res. 2009;105:365–74.
10. Hunter JP, Hosgood SA, Patel M, Rose R, Read K, Nicholson ML. Effects of hydrogen sulphide in an experimental model of renal ischaemia-reperfusion injury. Br J Surg. 2012;99:1665–71.
11. Fu Z, Liu X, Geng B, Fang L, Tang C. Hydrogen sulfide protects rat lung from ischemia-reperfusion injury. Life Sci. 2008;82:1196–202.
12. Henderson PW, Weinstein AL, Sohn AM, Jimenez N, Krijgh DD, Spector JA. Hydrogen sulfide attenuates intestinal ischemia-reperfusion injury when delivered in the post-ischemic period. J Gastroenterol Hepatol. 2010;25:1642–7.

13. Wang D, Ma Y, Li Z, Kang K, Sun X, Pan S, et al. The role of AKT1 and autophagy in the protective effect of hydrogen sulphide against hepatic ischemia/reperfusion injury in mice. Autophagy. 2012;8:954–62.
14. Jha S, Calvert JW, Duranski MR, Ramachandran A, Lefer DJ. Hydrogen sulfide attenuates hepatic ischemia-reperfusion injury: role of antioxidant and antiapoptotic signaling. Am J Physiol Heart Circ Physiol. 2008;295:H801–6.
15. Kang K, Zhao M, Jiang H, Tan G, Pan S, Sun X. Role of hydrogen sulfide in hepatic ischemia-reperfusion-induced injury in rats. Liver Transpl. 2009;15:1306–14.
16. Bos EM, Snijder PM, Jekel H, Weij M, Leemans JC, van Dijk MC, et al. Beneficial effects of gaseous hydrogen sulfide in hepatic ischemia/reperfusion injury. Transpl Int. 2012;25:897–908.
17. Kis A, Yellon DM, Baxter GF. Second window of protection following myocardial preconditioning: an essential role for PI3 kinase and p70S6 kinase. J Mol Cell Cardiol. 2003;35:1063–71.
18. Ban K, Kozar RA. Protective role of p70S6 K in intestinal ischemia/reperfusion injury in mice. PLoS One. 2012;7:e41584.
19. Lowicka E, Beltowski J. Hydrogen sulfide (H2S)—the third gas of interest for pharmacologists. Pharmacological reports. 2007;59:4–24.
20. Fukai M, Hayashi T, Yokota R, Shimamura T, Suzuki T, Taniguchi M, et al. Lipid peroxidation during ischemia depends on ischemia time in warm ischemia and reperfusion of rat liver. Free Radic Biol Med. 2005;38:1372–81.
21. Yadav SS, Gao W, Harland RC, Clavien PA. A new and simple technique of total hepatic ischemia in the mouse. Transplantation. 1998;65:1433–6.
22. Suzuki S, Nakamura S, Koizumi T, Sakaguchi S, Baba S, Muro H, et al. The beneficial effect of a prostaglandin I2 analog on ischemic rat liver. Transplantation. 1991;52:979–83.
23. Szabo C. Hydrogen sulphide and its therapeutic potential. Nat Rev Drug Discov. 2007;6:917–35.
24. Nakamitsu A, Hiyama E, Imamura Y, Matsuura Y, Yokoyama T. Kupffer cell function in ischemic and nonischemic livers after hepatic partial ischemia/reperfusion. Surg Today. 2001;31:140–8.
25. Schlegel A, Graf R, Clavien PA, Dutkowski P. Hypothermic oxygenated perfusion (HOPE) protects from biliary injury in a rodent model of DCD liver transplantation. J Hepatol. 2013;59:984–91.
26. Chen Y, Wood KJ. Interleukin-23 and TH17 cells in transplantation immunity: does 23 + 17 equal rejection? Transplantation. 2007;84:1071–4.
27. Husted TL, Blanchard J, Schuster R, Shen H, Lentsch AB. Potential role for IL-23 in hepatic ischemia/reperfusion injury. Inflamm Res. 2006;55:177–8.
28. Bhogal RH, Weston CJ, Curbishley SM, Adams DH, Afford SC. Activation of CD40 with platelet derived CD154 promotes reactive oxygen species dependent death of human hepatocytes during hypoxia and reoxygenation. PLoS One. 2012;7:e30867.
29. Ke B, Shen XD, Ji H, Kamo N, Gao F, Freitas MC, et al. HO-1-STAT3 axis in mouse liver ischemia/reperfusion injury: regulation of TLR4 innate responses through PI3 K/PTEN signaling. J Hepatol. 2011;56:359–66.
30. Shen X, Wang Y, Gao F, Ren F, Busuttil RW, Kupiec-Weglinski JW, et al. CD4 T cells promote tissue inflammation via CD40 signaling without de novo activation in a murine model of liver ischemia/reperfusion injury. Hepatology. 2009;50:1537–46.
31. Yokota R, Fukai M, Shimamura T, Suzuki T, Watanabe Y, Nagashima K, et al. A novel hydroxyl radical scavenger, nicaraven, protects the liver from warm ischemia and reperfusion injury. Surgery. 2000;127:661–9.
32. Ota T, Hirai R, Urakami A, Soga H, Nawa S, Shimizu N. Endothelin-1 levels in portal venous blood in relation to hepatic tissue microcirculation disturbance and hepatic cell injury after ischemia/reperfusion. Surg Today. 1997;27:313–20.
33. Johansen D, Ytrehus K, Baxter GF. Exogenous hydrogen sulfide (H2S) protects against regional myocardial ischemia-reperfusion injury–Evidence for a role of K ATP channels. Basic Res Cardiol. 2006;101:53–60.
34. Elrod JW, Calvert JW, Morrison J, Doeller JE, Kraus DW, Tao L, et al. Hydrogen sulfide attenuates myocardial ischemia-reperfusion injury by preservation of mitochondrial function. Proc Natl Acad Sci USA. 2007;104:15560–5.
35. Kimura Y, Goto Y, Kimura H. Hydrogen sulfide increases glutathione production and suppresses oxidative stress in mitochondria. Antioxid Redox Signal. 2010;12:1–13.
36. Paine A, Eiz-Vesper B, Blasczyk R, Immenschuh S. Signaling to heme oxygenase-1 and its anti-inflammatory therapeutic potential. Biochem Pharmacol. 2010;80:1895–903.
37. Kim YC, Yamaguchi Y, Kondo N, Masutani H, Yodoi J. Thioredoxin-dependent redox regulation of the antioxidant responsive element (ARE) in electrophile response. Oncogene. 2003;22:1860–5.
38. Akamatsu Y, Haga M, Tyagi S, Yamashita K, Graça-Souza AV, Ollinger R, et al. Heme oxygenase-1-derived carbon monoxide protects hearts from transplant associated ischemia reperfusion injury. Faseb J. 2004;18:771–2.
39. Wei Y, Chen P, de Bruyn M, Zhang W, Bremer E, Helfrich W. Carbon monoxide-releasing molecule-2 (CORM-2) attenuates acute hepatic ischemia reperfusion injury in rats. BMC Gastroenterol. 2010;10:42.
40. Watanabe R, Nakamura H, Masutani H, Yodoi J. Anti-oxidative, anti-cancer and anti-inflammatory actions by thioredoxin 1 and thioredoxin-binding protein-2. Pharmacol Ther. 2010;127:261–70.
41. Shao JL, Wan XH, Chen Y, Bi C, Chen HM, Zhong Y, et al. H_2S protects hippocampal neurons from anoxia-reoxygenation through cAMP-mediated PI3 K/Akt/p70S6 K cell-survival signaling pathways. J Mol Neurosci. 2011;43:453–60.
42. Si R, Tao L, Zhang HF, Yu QJ, Zhang R, Lv AL, et al. Survivin: a novel player in insulin cardioprotection against myocardial ischemia/reperfusion injury. J Mol Cell Cardiol. 2011;50:16–24.
43. Koh PO. Melatonin prevents hepatic injury-induced decrease in Akt downstream targets phosphorylations. J Pineal Res. 2011;51:214–9.
44. Debonera F, Wang G, Xie J, Que X, Gelman A, Leclair C, et al. Severe preservation injury induces Il-6/STAT3 activation with lack of cell cycle progression after partial liver graft transplantation. Am J Transplant. 2004;4:1964–71.
45. Taub R. Liver regeneration: from myth to mechanism. Nat Rev Mol Cell Biol. 2004;5:836–47.
46. Zhang Q, Fu H, Zhang H, Xu F, Zou Z, Liu M, et al. Hydrogen sulfide preconditioning protects rat liver against ischemia/reperfusion injury by activating Akt-GSK-3β signaling and inhibiting mitochondrial permeability transition. PLoS One. 2013;8:e74422.
47. Klingerman CM, Trushin N, Prokopczyk B, Haouzi P. H_2S concentrations in the arterial blood during H_2S administration in relation to its toxicity and effects on breathing. Am J Physiol Regul Integr Comp Physiol. 2013;305:R630–8.
48. Vitvitsky V, Kabil O, Banerjee R. High turnover rates for hydrogen sulfide allow for rapid regulation of its tissue concentrations. Antioxid Redox Signal. 2012;17:22–31.
49. Balaban CL, Rodriguez JV, Guibert EE. Delivery of the bioactive gas hydrogen sulfide during cold preservation of rat liver: effects on hepatic function in an ex vivo model. Artif Organs. 2011;35:508–15.

Cancer Science
Japanese Cancer Association JCA
Open Access

Suprabasin as a novel tumor endothelial cell marker

Mohammad T. Alam,[1,2,6] Hiroko Nagao-Kitamoto,[1,6] Noritaka Ohga,[1] Kosuke Akiyama,[1] Nako Maishi,[1] Taisuke Kawamoto,[1] Nobuo Shinohara,[3] Akinobu Taketomi,[4] Masanobu Shindoh,[2] Yasuhiro Hida[5] and Kyoko Hida[1]

[1]Vascular Biology, Frontier Research Unit, Institute for Genetic Medicine, Hokkaido University, Sapporo; [2]Department of Oral Pathology and Biology, Graduate School of Dental Medicine, Hokkaido University, Sapporo; Departments of [3]Renal and Genitourinary Surgery; [4]Gastroenterological Surgery I; [5]Cardiovascular and Thoracic Surgery, Graduate School of Medicine, Hokkaido University, Sapporo, Japan

Key words

Angiogenesis, suprabasin, suprabasin signaling, tumor endothelial cell marker, tumor endothelial cells

Correspondence

Kyoko Hida, Vascular Biology, Frontier Research Unit, Institute for Genetic Medicine, Hokkaido University, N15, W7, Kita-Ku, Sapporo 060-0815, Japan.
Tel: +81-11-706-4315; Fax: +81-11-706-4325;
E-mail: khida@igm.hokudai.ac.jp

[6]These authors contributed equally to this manuscript.

Funding Information

This article was supported in part by a Grant-in-Aid for scientific research from the Ministry of Education, Science and Culture of Japan (20390506 and 23112501 to Kyoko Hida). The funders had no role in study design, data collection and analysis, decision to publish, or preparation of the manuscript.

Received June 3, 2014; Revised September 26, 2014; Accepted September 30, 2014

Cancer Sci **105** (2014) 1533–1540

doi: 10.1111/cas.12549

Recent studies have reported that stromal cells contribute to tumor progression. We previously demonstrated that tumor endothelial cells (TEC) characteristics were different from those of normal endothelial cells (NEC). Furthermore, we performed gene profile analysis in TEC and NEC, revealing that suprabasin (SBSN) was upregulated in TEC compared with NEC. However, its role in TEC is still unknown. Here we showed that SBSN expression was higher in isolated human and mouse TEC than in NEC. SBSN knockdown inhibited the migration and tube formation ability of TEC. We also showed that the AKT pathway was a downstream factor of SBSN. These findings suggest that SBSN is involved in the angiogenic potential of TEC and may be a novel TEC marker.

Tumor angiogenesis is necessary for the progression of tumor growth and metastasis.[1,2] Because tumor blood vessels supply tumor cells with nutrients and oxygen, anti-angiogenesis treatment is recognized as a new cancer therapy.[3] Bevacizumab, anti-vascular endothelial growth factor (VEGF) antibody,[4] and sorafenib or sunitinib, a VEGF receptor kinase inhibitor, have been used as anti-angiogenic drugs.[5] However, there are negative reports regarding side effects and increases in metastasis have been observed. To overcome these problems, a new anti-angiogenic drug is required.[6] The morphology of tumor blood vessels is different from that of normal blood vessels.[7–9] Differences between tumor endothelial cells (TEC) and normal endothelial cells (NEC) in aspects, such as gene expression and biological behavior, have also been reported.[7,8,10] Recently, we revealed that TEC were more resistant to anti-cancer drugs compared with NEC.[11] In addition, inhibition of cyclooxygenase-2 or lysyl oxidase in TEC suppressed tumor growth and lung metastasis *in vivo*.[12,13] These findings indicate that TEC may be a good target for anti-cancer therapy. To identify specific TEC markers, we performed DNA microarray analysis and reported that some molecules were upregulated in TEC.[14–16] Among these molecules, suprabasin (SBSN) showed very high expression levels in several TEC.

Suprabasin has been identified as an epidermal differentiation marker and has been detected in the suprabasal layers of the epithelia in the epidermis, stomach and tongue in mice.[17,18] SBSN participates in the proliferation of normal small cell lung carcinoma cells.[19] The SBSN expression is also correlated with the growth and invasiveness of salivary gland adenoid cystic carcinoma and glioblastoma.[20,21] However, the details of SBSN's involvement in tumor malignancy and tumor angiogenesis are unknown.

In this study, we examined the SBSN expression and its function in TEC to determine whether SBSN is a potential TEC marker.

Materials and Methods

Cell lines and culture conditions. The human renal clear cell carcinoma cell OS-RC-2 was purchased from the RIKEN Cell Bank (Tsukuba, Japan) and cultured in RPMI1640 medium (Sigma–Aldrich, St. Louis, MO, USA) supplemented with 10% heat-inactivated FBS, 100 U/mL penicillin and 100 μg/mL streptomycin. A375SM cells, a super-metastatic human melanoma cell line, were a gift from Dr Isaiah J Fidler (MD Anderson Cancer Center, Houston, TX, USA). The cells were cultured in minimum essential medium (Gibco, Grand Island, NY, USA) supplemented with 10% FBS, 100 U/mL penicillin and 100 μg/mL

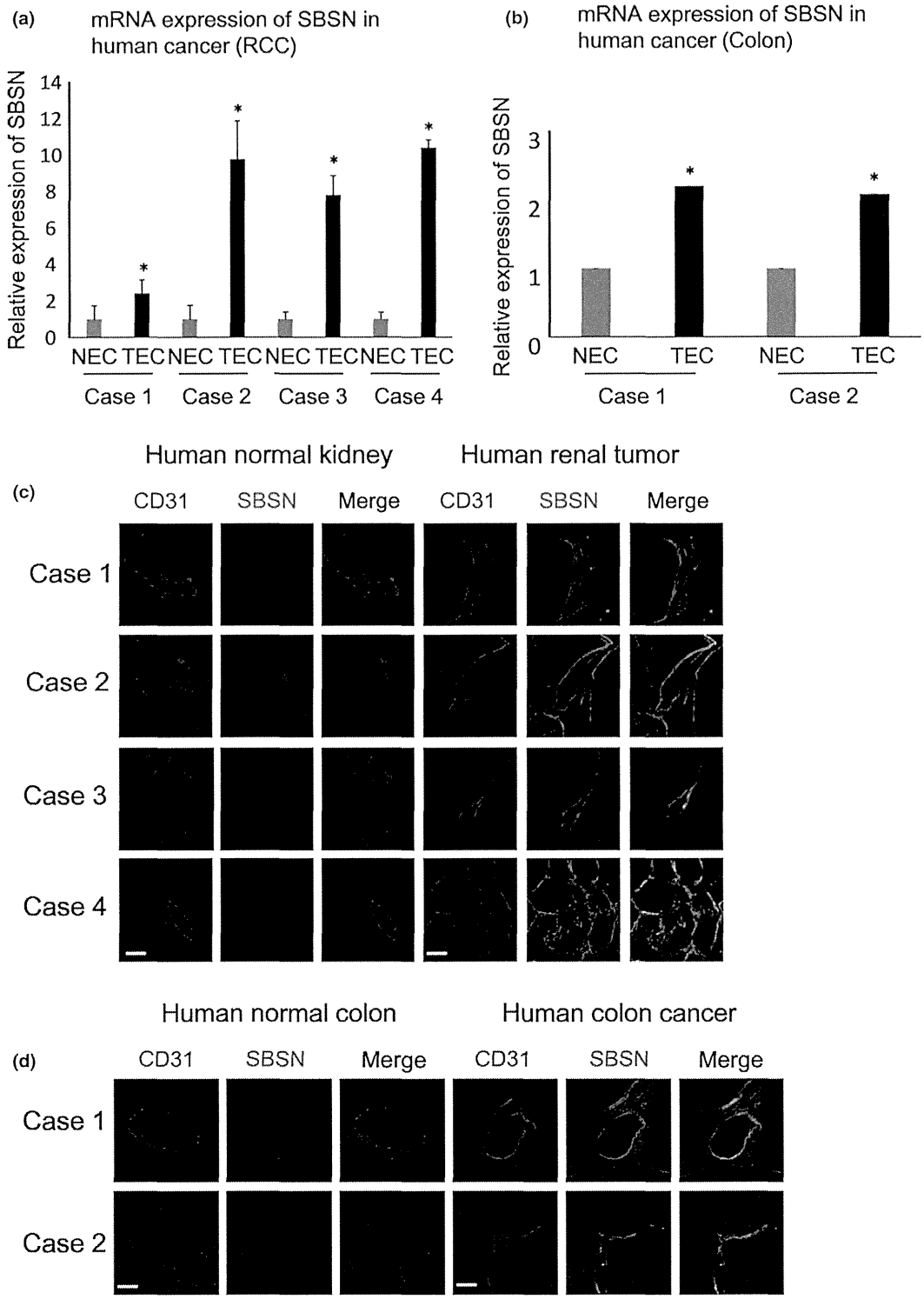

Fig. 1. Suprabasin (SBSN) expression in human tumor endothelial cells (hTEC). (a, b) Relative *SBSN* mRNA expression levels in hNEC and hTEC evaluated by quantitative PCR (a, RCC, $n = 4$; b, colon tumor, $n = 2$). *$P < 0.01$ versus control; two-sided Student's *t*-test. (c, d) Clinical samples of renal cell carcinoma (RCC) and colon cancer-derived tumor endothelial cells were double-stained with anti-CD31 and anti-SBSN antibodies. Scale bar: 50 μm.

streptomycin, as described previously.[15] In the growth factor experiments, NEC were treated with human EGF (AF-100-15; PeproTech, Rocky Hill, NJ, USA) at final concentrations of 5 and 15 ng/mL and human VEGF (100-20; PeproTech, Rocky Hill, NJ, USA) at final concentrations of 15 and 30 ng/mL for 12 h. These cells were cultured at 37°C in a humidified atmosphere of 5% CO_2 and 95% air.

Isolation of tumor endothelial cells and normal endothelial cells. All procedures for animal experiments were approved by the local animal research authorities, and animal care

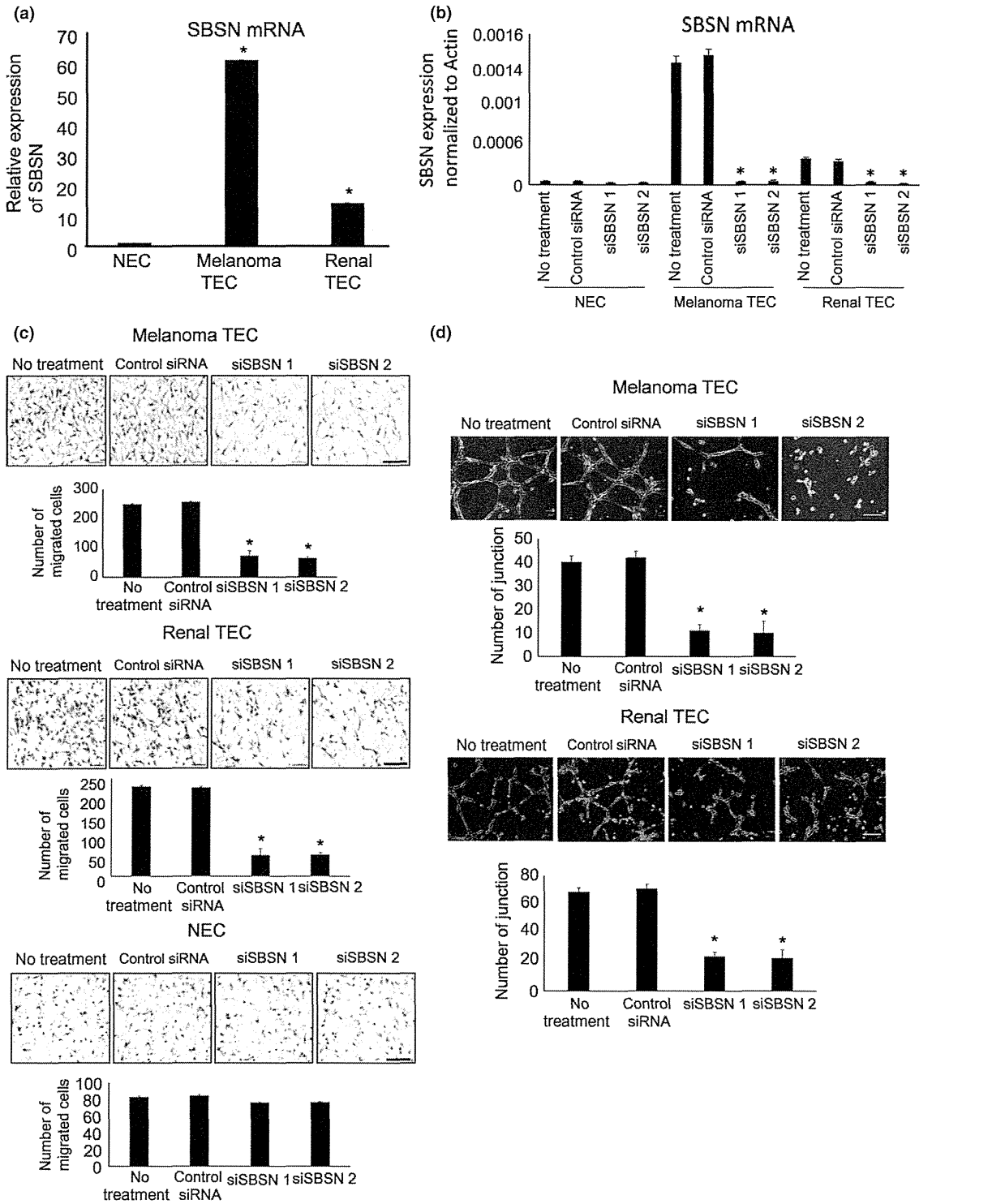

Fig. 2. Effect of *SBSN* knockdown on cell migration and tube formation in mouse tumor endothelial cells (mTEC). (a) Relative *SBSN* mRNA expression levels in mouse normal endothelial cells (mNEC) and mTEC (melanoma and renal) evaluated by quantitative PCR. (b) *SBSN* mRNA expression levels in mTEC and mNEC transfected with the control siRNA or si*SBSN*, determined by quantitative PCR. (c) Migration toward vascular endothelial growth factor (VEGF) of mTEC and mNEC transfected with control siRNA or si*SBSN* analyzed using a Boyden chamber. Scale bar: 100 μm. (d) Tube number of mTEC transfected with control siRNA or si*SBSN*. Scale bar: 50 μm. *$P < 0.01$ versus control; one-way ANOVA with the Tukey–Kramer multiple comparison test (mean ± SD, $n = 3$).

was performed in accordance with institutional guidelines. Mouse TEC (mTEC) and NEC (mNEC) were isolated as previously described[12] with some modifications. Diphtheria toxin (500 ng/mL; Calbiochem, San Diego, CA, USA) was added to mTEC subcultures to kill any human tumor cells and to mNEC subcultures for technical consistency. Using

an anti-human CD31 antibody, human TEC (hTEC) and NEC (hNEC) were isolated from excised renal cell carcinoma (RCC) or colon cancer tissues from patients at Hokkaido University Hospital. Normal renal or colon tissues were obtained from areas that were adjacent to the tumor in the same patient. Clinical background information is described

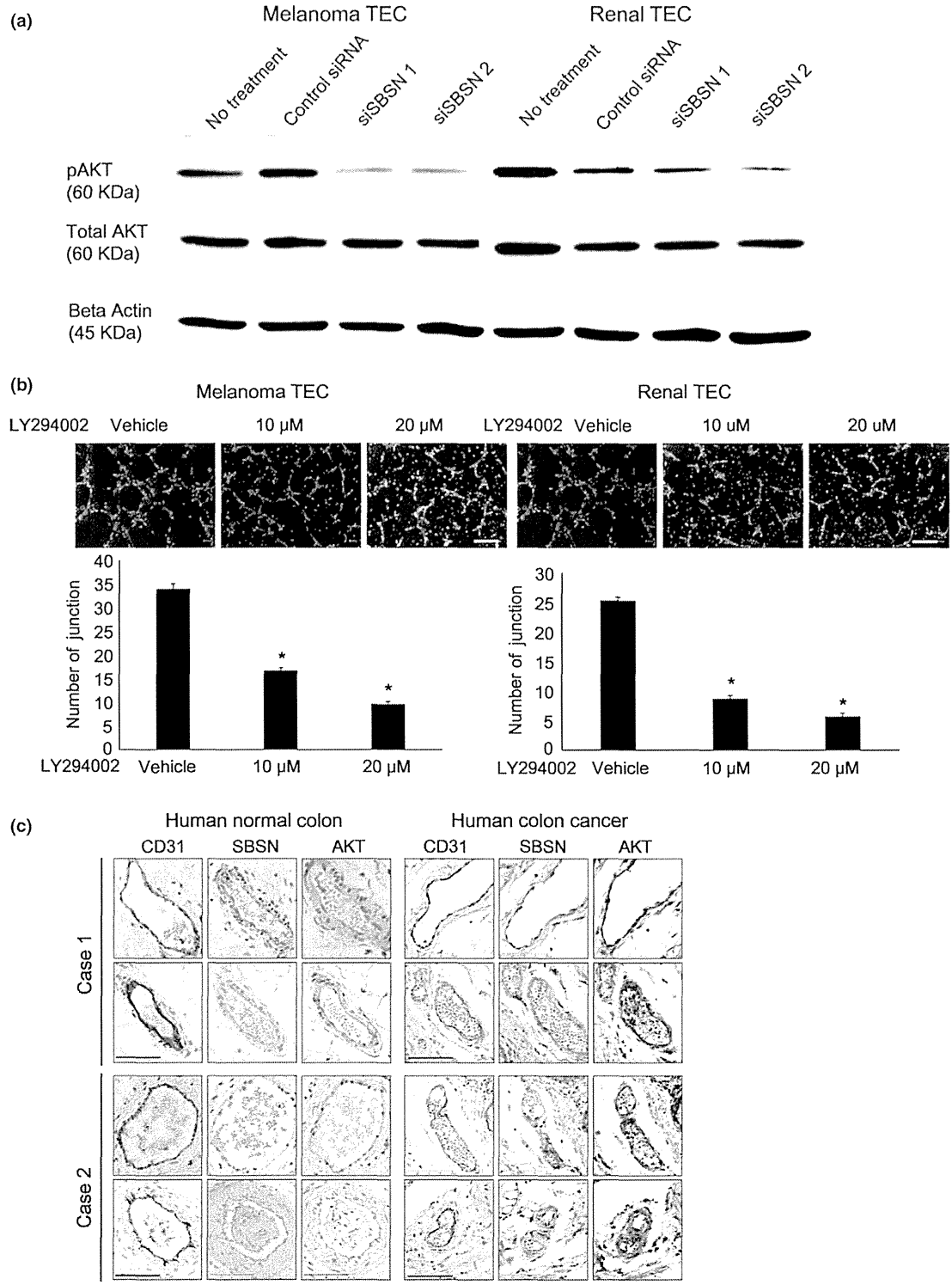

Fig. 3. Relationship between suprabasin (SBSN) knockdown and AKT activation in mouse tumor endothelial cells (mTEC) *in vitro* and *in vivo*. (a) Total AKT, phosphorylated AKT (p-AKT), and beta actin protein levels in mTEC treated with control siRNA or si*SBSN*, determined by western blotting. (b) Tube number of mTEC treated with or without LY294002 (10 or 20 μM) evaluated by the tube formation assay. Scale bar: 100 μm. *$P < 0.05$ versus control; two-sided Student's *t*-test (mean ± SD, $n = 3$). (c) SBSN and AKT expression levels were determined by immunohistochemical analysis. CD31-positive blood vessels were stained with anti-SBSN and anti-AKT antibodies in two cases of human colon cancer (Cases 1 and 2), whereas those of normal tissues were weakly stained *in vivo*. Scale bar: 80 μm.

in Supplementary Table S1. These protocols were approved by the Ethics Committee of Hokkaido University, and written informed consent was obtained from each patient before surgery. Endothelial cells (EC) were cultured as previously described.[22,23]

Reverse transcription and quantitative PCR. Total RNA was extracted from cells and human tumor and normal tissue samples using the ReliaPrep RNA Cell Miniprep System (Promega Corporation, Madison, WI, USA). Complementary DNA (cDNA) was synthesized using a ReverTra-Plus kit (Toyobo, Osaka, Japan). For relative quantification of target mRNA, we used SsoFast EvaGreen Supermix (CFX 96 Real-Time PCR Detection System; Bio-Rad, Hercules, CA, USA) for mouse EC and SYBR Green Real-time PCR Master Mix-Plus (Bio-Rad) for human EC (in triplicate) according to the manufacturer's instructions.[24] The quantitative PCR amplification program was performed at 95°C for 3 min and 45 cycles at 95°C for 10 s and 60°C for 30 s. Data were analyzed with CFX Manager software (Bio-Rad). The primers used are described in Supplementary Table S2. Each experiment included four PCR reactions, and each experiment was performed three times.

Western blotting. Western blotting analysis was performed as described previously.[25] This analysis used antibodies specific for total AKT, phosphorylated AKT (Cell Signaling Technology, Beverly, MA, USA), total Erk, phosphorylated Erk (Cell Signaling Technology), beta actin and an HRP-conjugated secondary antibody.

Immunostaining. Human tissue samples were obtained from excised RCC, normal renal tissue, colon cancer and normal colon tissues of patients at Hokkaido University Hospital. Frozen sections of excised tissues were prepared as previously described.[14,26] Human sections were double-stained with anti-human CD31/Alexa Fluor 594 rat anti-mouse IgG and anti-SBSN/Alexa Fluor 488 goat anti-rabbit IgG. All samples were counterstained with DAPI (Roche Diagnostics, Mannheim, Germany) and examined using an Olympus FluoView FV10i confocal microscope (Olympus, Tokyo, Japan).

For AKT staining, formalin-fixed paraffin-embedded specimens from two cases of colon cancer were prepared. Immunohistochemical analysis was performed using serial sections that were stained with anti-SBSN (1:250 dilution), AKT (1:100 dilution) and CD31 (Leica Microsystem, UK; 1:500 dilution), followed by antibody detection using a peroxidase-conjugated streptavidin-diaminobenzidine (DAB) readout system (DAKO), and counterstaining with DAPI. Images were randomly captured using a nanozoomer slide scanner and NDPViewer (Hamamatsu, Japan).

Suprabasin knockdown. si*SBSN* was transfected into cells using Lipofectamine transfection reagent (Invitrogen, Tokyo, Japan) according to the manufacturer's instructions. The sequence of si*SBSN* was 5′-UAUUGAUGCCUUCAA GGGCCUUGCC-3′ (siSBSN1) and 5′-UUCCCUUCCAGCU UGAGUGAUUCCG-3′ (siSBSN2). A nontargeting control siRNA was used (Invitrogen).

Cell migration assay. Cell migration toward VEGF-A was analyzed using a Boyden chamber (Neuro Probe, Gaithersburg, MD, USA), as previously described.[27] VEGF-A (10 ng/mL) was added to the lower chamber as a chemoattractant. TEC were treated with the control siRNA (10 nM) or si*SBSN* (10 nM) in endothelial basal medium (EBM)-2 supplemented with 0.5% FBS for 24 h. In total, 1.5×10^4cells were seeded in the upper chamber and

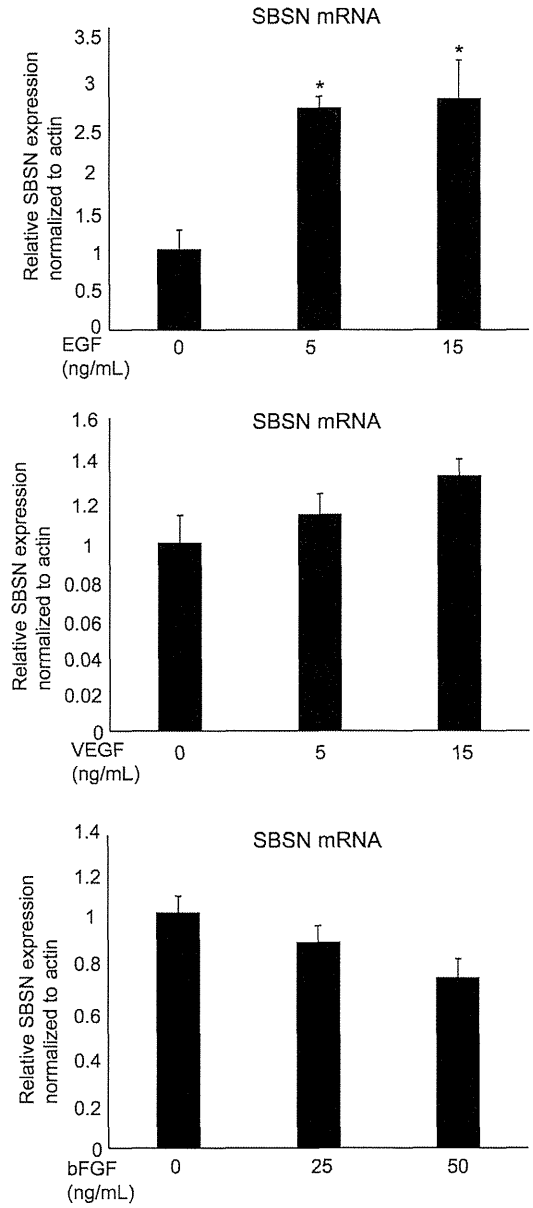

Fig. 4. Suprabasin (SBSN) expression after growth factor treatment. NEC were incubated in 0.5% EBM2 medium for 12 h, followed by treatment with endothelial growth factor (EGF), vascular endothelial growth factor (VEGF) and basic fibroblast growth factor (bFGF) for 12 h. The cells were cultured at 37°C in a humidified atmosphere of 5% CO_2. *$P < 0.05$ versus control; two-sided student's *t*-test. After 12 h of incubation, mRNA was extracted from the cells and used in the RT-PCR analysis of SBSN expression.

incubated for 4 h at 37°C. The assays were independently performed three times.

Tube formation assay. A tube formation assay was performed as previously described.[26] EC were seeded at a density of 1.0×10^5 cells per well and incubated at 37°C on Matrigel (BD Biosciences, San Jose, CA, USA). Tube formation was observed using an inverted microscope by measuring the junction number of endothelial tubes. For inhibition experiments using the PI3 kinase inhibitor LY294002, TEC were preincubated for 2 h at 37°C in EBM2 supplemented with 0.5% FBS. To investigate the involvement of AKT in TEC tube formation, assays were performed with or without LY294002 (0, 10

or 20 μM). The assays were independently performed three times.

Cell proliferation assay. Cell proliferation was assessed with an MTS assay as described previously.[11] TEC were treated with the control siRNA (10 nM) or si*SBSN* (10 nM) in EBM2 supplemented with 0.5% FBS for 24 h. After siRNA transfection, 1.0×10^3 cells per well were seeded into 96-well plates in EBM2 supplemented with 5% FBS. Cell proliferation was measured daily for 3 days by the MTS assay. The assays were independently performed three times.

Statistical analysis. Results are given as mean ± SD. Group comparisons were made by one-way ANOVA with the Tukey–Kramer multiple comparison test. When only two groups were compared, a two-sided Student's *t*-test was used. $P < 0.05$ was considered significant, and $P < 0.01$ was considered highly significant.

Results

Suprabasin was highly expressed in human tumor endothelial cells. To analyze the SBSN expression in hTEC and hNEC, we isolated hTEC from tissues of four cases of RCC and two cases of colon cancer. Furthermore, hNEC were isolated from the tissues of normal renal tissue and colon in the same patients.[14,28] The *SBSN* mRNA expression levels in hTEC isolated from RCC and colon cancer tissues were higher than those of hNEC (Fig. 1a,b). Double-immunofluorescence staining with anti-SBSN and anti-CD31 antibodies revealed that SBSN was markedly expressed in tumor blood vessels both in RCC and colon cancer, whereas the SBSN expression was low in normal blood vessels (Fig. 1c,d). In addition, SBSN mRNA expression levels were higher in human renal tumor tissues than those in normal tissues (Suppl. Fig. S1). These findings showed that SBSN was upregulated in hTEC from several tumor types.

Suprabasin knockdown inhibited migration and tube formation of mouse tumor endothelial cells. To clarify the role of SBSN in TEC, we used mTEC isolated from human tumor xenografts (A375SM and OS-RC-2). mNEC were isolated from mouse dermis as a normal control. We verified that mNEC and mTEC had the characteristics of EC using an RT-PCR assay (Suppl. Fig. S2). The *SBSN* mRNA expression levels were upregulated in mTEC from melanoma and renal carcinoma compared with mNEC (Fig. 2a) and other mouse normal tissues (Suppl. Fig. S3). To evaluate the SBSN function in TEC, we examined the migration ability and tube formation of mTEC following the *SBSN* knockdown. The efficacy of RNA interference (RNAi) was confirmed using quantitative real-time PCR, which showed that si*SBSN*, unlike control siRNA, decreased the SBSN mRNA level in mTEC and mNEC (Fig. 2b). We next demonstrated that the *SBSN* knockdown significantly suppressed cell migration toward VEGF-A in mTEC but not in mNEC (Fig. 2c). However, siSBSN had no effect on cell proliferation in either mTEC or mNEC (Suppl. Fig. S4). In this study, we used two types of siRNA and obtained similar results. This suggests that the results are not off-target effects of the nucleic acids. In addition, the junction number of endothelial tubes in mTEC was reduced by si*SBSN* treatment (Fig. 2d). These findings revealed that SBSN contributed to the angiogenic phenotype, such as migration and tube formation in mTEC.

Suprabasin knockdown suppressed AKT pathway in mouse tumor endothelial cells. The PI3K/AKT pathway plays an essential role in the survival of TEC.[29] We previously reported that activation of AKT was involved in cell migration of mTEC;[13,23] and, therefore, we explored the interaction between the AKT pathway and SBSN. Phosphorylation of AKT in mTEC was suppressed by the PI3K inhibitor LY294002 treatment (Suppl. Fig. S5a). Moreover, we showed that the protein level of phosphorylated AKT was reduced by si*SBSN* treatment compared with control siRNA in both types of mTEC (melanoma and renal) (Fig. 3a), but not in NEC or in other cell types (Suppl. Fig. S5b). Moreover, we demonstrated that LY294002 inhibited tube formation in mTEC in a concentration-dependent manner (Fig. 3b). These findings indicate that SBSN regulated the migration and tube formation of mTEC via the AKT pathway. In addition, SBSN-positive blood vessels in human colon cancer tissues were positively stained by anti-AKT, but not those of normal colon tissues (Fig. 3c). This result suggests that SBSN may also be involved in AKT activation in human tumor blood vessels. To address how SBSN expression is regulated, endothelial cells were treated with growth factors such as endothelial growth factor (EGF), VEGF and fibroblast growth factor-2 (FGF-2). Among these growth factors, EGF significantly induced SBSN mRNA expression in NEC (Fig. 4).

Discussion

In this study, we demonstrated that the SBSN expression was markedly increased in human TEC (renal carcinoma and colon carcinomas) as well as mTEC (melanoma and renal carcinoma). These findings indicate that SBSN may be used as a common marker of TEC.

The *SBSN* mRNA expression levels tended to be higher in hTEC (isolated from renal carcinoma) with higher T classifications under the tumor-node-metastasis system (order: case 4 > 2 > 3 > 1) (Suppl. Table S1). In this study, because the number of clinical samples was small, further studies are required to explore the relationship between the SBSN expression and clinical background in larger numbers of patients.

Previously, we reported that mTEC demonstrate a pro-angiogenic phenotype compared with mNEC.[11,30,31] SBSN plays a role in epidermal differentiation[18] and the growth and invasiveness of tumors.[19–21] For example, Shao *et al.*[21] report that SBSN was upregulated because the SBSN gene promoter in adenocystic carcinoma was demethylated. However, our preliminary analysis of epigenetics showed that methylation levels in TEC did not differ from those in NEC, which suggests that there may be another mechanism that is responsible for the enhanced expression of the *SBSN* gene in TEC. We found that EGF upregulated the expression of SBSN in NEC. However, its mechanism of transcriptional regulation or its function in tumor angiogenesis is unknown. In this study, we demonstrated that the *SBSN* knockdown inhibited cell migration and tube formation in mTEC. These findings revealed the role of SBSN in tumor angiogenesis.

We previously reported that the VEGF receptor-2 (VEGFR-2) expression was high in TEC and that TEC were more sensitive to VEGF than NEC.[27] The *SBSN* knockdown had no significant effect on the *VEGFR* mRNA expression in mTEC, suggesting that involvement of SBSN in the angiogenic phenotype of mTEC is independent of VEGF/VEGFR-2 signaling.

There has been no report of SBSN signaling. We showed that the activation of AKT was suppressed by siSBSN. However, activation of the ERK pathway, which is related to angiogenesis, was not affected (Suppl. Fig. S6). Our finding revealed at least a part of downstream signaling of SBSN in TEC. Thus, these findings enhanced our understanding of TEC function.

Our data demonstrate that the number of tube junctions in TEC was decreased more by si*SBSN* than by a PI3K inhibitor.

These results suggest that other molecules besides AKT are involved in SBSN-related tube formation in mTEC. Additional studies are required to determine whether the AKT is directly involved in the downstream of SBSN.

In this study, to the best of our knowledge, we demonstrated for the first time that SBSN is upregulated in TEC and that SBSN plays significant roles in the pro-angiogenic phenotype in TEC, but not in NEC. In this study, we showed that SBSN could be a potential TEC marker. Thus, SBSN may be a novel target for anti-angiogenic therapy, which is specific for tumor blood vessels.

Acknowledgments

We thank Dr I. J. Fidler for providing the A375SM super-metastatic human malignant melanoma cell line and Dr Aya Matsuda, Ms. Yuko Suzuki, and Ms. Tomomi Takahashi for their technical assistance in the experiments. This article was supported in part by a Grant-in-Aid for scientific research from the Ministry of Education, Science and Culture of Japan (20390506 and 23112501 to Kyoko Hida). The funders had no role in study design, data collection and analysis, decision to publish, or preparation of the manuscript.

Disclosure Statement

The authors have no conflict of interest to declare.

References

1 Folkman J. Role of angiogenesis in tumor growth and metastasis. *Semin Oncol* 2002; **29**: 15–8.
2 Folkman J. Angiogenesis: an organizing principle for drug discovery? *Nat Rev Drug Discov* 2007; **6**: 273–86.
3 Welti J, Loges S, Dimmeler S, Carmeliet P. Recent molecular discoveries in angiogenesis and antiangiogenic therapies in cancer. *J Clin Invest* 2013; **123**: 3190–200.
4 Willett CG, Boucher Y, di Tomaso E *et al.* Direct evidence that the VEGF-specific antibody bevacizumab has antivascular effects in human rectal cancer. *Nat Med* 2004; **10**: 145–7.
5 Ivy SP, Wick JY, Kaufman BM. An overview of small-molecule inhibitors of VEGFR signaling. *Nat Rev Clin Oncol* 2009; **6**: 569–79.
6 Jain RK, Duda DG, Clark JW, Loeffler JS. Lessons from phase III clinical trials on anti-VEGF therapy for cancer. *Nat Clin Pract Oncol* 2006; **3**: 24–40.
7 McDonald DM, Baluk P. Significance of blood vessel leakiness in cancer. *Cancer Res* 2002; **62**: 5381–5.
8 Morikawa S, Baluk P, Kaidoh T, Haskell A, Jain RK, McDonald DM. Abnormalities in pericytes on blood vessels and endothelial sprouts in tumors. *Am J Pathol* 2002; **160**: 985–1000.
9 Jain RK. Molecular regulation of vessel maturation. *Nat Med* 2003; **9**: 685–93.
10 St Croix B, Rago C, Velculescu V *et al.* Genes expressed in human tumor endothelium. *Science* 2000; **289**: 1197–202.
11 Akiyama K, Ohga N, Hida Y *et al.* Tumor endothelial cells acquire drug resistance by MDR1 up-regulation via VEGF signaling in tumor microenvironment. *Am J Pathol* 2012; **180**: 1283–93.
12 Osawa T, Ohga N, Akiyama K *et al.* Lysyl oxidase secreted by tumour endothelial cells promotes angiogenesis and metastasis. *Br J Cancer* 2013; **109**: 2237–47.
13 Muraki C, Ohga N, Hida Y *et al.* Cyclooxygenase-2 inhibition causes antiangiogenic effects on tumor endothelial and vascular progenitor cells. *Int J Cancer* 2012; **130**: 59–70.
14 Maishi N, Ohga N, Hida Y *et al.* CXCR7: a novel tumor endothelial marker in renal cell carcinoma. *Pathol Int* 2012; **62**: 309–17.
15 Osawa T, Ohga N, Hida Y *et al.* Prostacyclin receptor in tumor endothelial cells promotes angiogenesis in an autocrine manner. *Cancer Sci* 2012; **103**: 1038–44.
16 Yamamoto K, Ohga N, Hida Y *et al.* Biglycan is a specific marker and an autocrine angiogenic factor of tumour endothelial cells. *Br J Cancer* 2012; **106**: 1214–23.
17 Matsui T, Hayashi-Kisumi F, Kinoshita Y *et al.* Identification of novel keratinocyte-secreted peptides dermokine-alpha/-beta and a new stratified epithelium-secreted protein gene complex on human chromosome 19q13.1. *Genomics* 2004; **84**: 384–97.
18 Park GT, Lim SE, Jang SI, Morasso MI. Suprabasin, a novel epidermal differentiation marker and potential cornified envelope precursor. *J Biol Chem* 2002; **277**: 45195–202.
19 Glazer CA, Smith IM, Ochs MF *et al.* Integrative discovery of epigenetically derepressed cancer testis antigens in NSCLC. *PLoS ONE* 2009; **4**: e8189.
20 Formolo CA, Williams R, Gordish-Dressman H, MacDonald TJ, Lee NH, Hathout Y. Secretome signature of invasive glioblastoma multiforme. *J Proteome Res* 2011; **10**: 3149–59.
21 Shao C, Tan M, Bishop JA *et al.* Suprabasin is hypomethylated and associated with metastasis in salivary adenoid cystic carcinoma. *PLoS ONE* 2012; **7**: e48582.
22 Akino T, Hida K, Hida Y *et al.* Cytogenetic abnormalities of tumor-associated endothelial cells in human malignant tumors. *Am J Pathol* 2009; **175**: 2657–67.
23 Ohga N, Hida K, Hida Y *et al.* Inhibitory effects of epigallocatechin-3 gallate, a polyphenol in green tea, on tumor-associated endothelial cells and endothelial progenitor cells. *Cancer Sci* 2009; **100**: 1963–70.
24 Kondoh M, Ohga N, Akiyama K *et al.* Hypoxia-induced reactive oxygen species cause chromosomal abnormalities in endothelial cells in the tumor microenvironment. *PLoS ONE* 2013; **8**: e80349.
25 Kawamoto T, Ohga N, Akiyama K *et al.* Tumor-derived microvesicles induce proangiogenic phenotype in endothelial cells via endocytosis. *PLoS ONE* 2012; **7**: e34045.
26 Kurosu T, Ohga N, Hida Y *et al.* HuR keeps an angiogenic switch on by stabilising mRNA of VEGF and COX-2 in tumour endothelium. *Br J Cancer* 2011; **104**: 819–29.
27 Matsuda K, Ohga N, Hida Y *et al.* Isolated tumor endothelial cells maintain specific character during long-term culture. *Biochem Biophys Res Commun* 2010; **394**: 947–54.
28 Akiyama K, Ohga N, Maishi N *et al.* The F-prostaglandin receptor is a novel marker for tumor endothelial cells in renal cell carcinoma. *Pathol Int* 2013; **63**: 37–44.
29 Bussolati B, Deambrosis I, Russo S, Deregibus MC, Camussi G. Altered angiogenesis and survival in human tumor-derived endothelial cells. *FASEB J* 2003; **17**: 1159–61.
30 Hida K, Hida Y, Amin DN *et al.* Tumor-associated endothelial cells with cytogenetic abnormalities. *Cancer Res* 2004; **64**: 8249–55.
31 Ohga N, Ishikawa S, Maishi N *et al.* Heterogeneity of tumor endothelial cells: comparison between tumor endothelial cells isolated from high- and low-metastatic tumors. *Am J Pathol* 2012; **180**: 1294–307.

Supporting Information

Additional supporting information may be found in the online version of this article:

Fig. S1. Suprabasin (SBSN) expression in human tumor tissues. Relative *SBSN* mRNA expression levels in both human colon normal and cancer tissues were analyzed by quantitative RT-PCR. $*P < 0.05$ versus control; two-sided Student's *t*-test. Clinical samples from three patients were collected.

Fig. S2. Characterization of isolated mouse tumor endothelial cells (mTEC) and mouse normal endothelial cells (mNEC). mRNA levels of CD31, CD105, VEGFR-1 (VR1), VEGFR-2 (VR2), CD11b, CD45, human HB-EGF (hHB-EGF) and GAPDH in mTEC and mNEC were evaluated by RT-PCR.

Fig. S3. SBSN expression in mouse tumor endothelial cells (mTEC) and other various tissue of mouse organs. Relative *SBSN* mRNA expression levels in various tissue of mouse organs besides ECs analyzed by quantitative PCR. $*P < 0.01$ versus control. (ND, not detected.)

Fig. S4. Effect of si*SBSN* on proliferation of mouse tumor endothelial cells (mTEC) transfected with control siRNA or si*SBSN* was analyzed using the MTS assay.

Fig. S5. (a) Effect of LY294002 treatment on mouse tumor endothelial cells (mTEC). (a) Total AKT, phosphorylated AKT (p-AKT), and beta actin protein levels in mTEC treated or not treated with LY294002 (10 or 20 μM) were determined by western blotting. (b) Total AKT, phosphorylated AKT (p-AKT), and beta actin protein levels in mTEC were compared with those of the NEC, NIH3T3 and B16F10 cell lines transfected with control siRNA or si*SBSN*. Approximately 20 μg of total protein was loaded into each lane for western blot analysis.

Fig. S6. Effect of ERK activation by suprabasin (SBSN) knockdown. ERK activation was determined by western blot analysis. Total ERK and phosphorylated ERK (p-ERK) protein expression levels were detected in mouse tumor endothelial cells (mTEC) transfected with control siRNA or si*SBSN* in melanoma tumor endothelial cells (TEC) and renal TEC. Approximately 20 μg of total protein was loaded into each lane for western blot analysis. Beta actin antibody was used as internal control.

Table S1. Clinical background of renal cell carcinoma (RCC) and colon cancer specimens. M/F, male/female; †according to 1997 tumor-node-metastasis (TNM) staging guidelines; ††according to the Fuhrman system.

Table S2. List of primers. Primer sequences for RT-PCR and quantitative PCR.

THE JOURNAL OF BIOLOGICAL CHEMISTRY VOL. 289, NO. 38, pp. 26607–26617, September 19, 2014

Diacylglycerol Kinase δ Phosphorylates Phosphatidylcholine-specific Phospholipase C-dependent, Palmitic Acid-containing Diacylglycerol Species in Response to High Glucose Levels*

Received for publication, June 20, 2014, and in revised form, August 8, 2014 Published, JBC Papers in Press, August 11, 2014, DOI 10.1074/jbc.M114.590950

Hiromichi Sakai[‡], **Sayaka Kado**[§], **Akinobu Taketomi**[¶], **and Fumio Sakane**[‡1]

From the [‡]*Department of Chemistry, Graduate School of Science and* [§]*Center for Analytical Instrumentation, Chiba University, 1-33 Yayoi-cho, Inage-ku, Chiba 263-8522 and the* [¶]*Department of General Surgery, Graduate School of Medicine, Hokkaido University, North 15, West 7, Kita-ku, Sapporo 060-8638, Japan*

Background: Diacylglycerol (DG) kinase (DGK) δ is activated by acute high glucose stimulation.
Results: DGKδ high glucose-dependently phosphorylates 30:0-, 32:0-, and 34:0-DG and interacts with phosphatidylcholine-specific phospholipase C (PC-PLC).
Conclusion: DGKδ utilizes palmitic acid-containing DG species and metabolically connects with PC-PLC.
Significance: The newly identified PC-PLC/DGKδ pathway could play an important role in insulin signaling and glucose uptake.

Decreased expression of diacylglycerol (DG) kinase (DGK) δ in skeletal muscles is closely related to the pathogenesis of type 2 diabetes. To identify DG species that are phosphorylated by DGKδ in response to high glucose stimulation, we investigated high glucose-dependent changes in phosphatidic acid (PA) molecular species in mouse C2C12 myoblasts using a newly established liquid chromatography/MS method. We found that the suppression of DGKδ2 expression by DGKδ-specific siRNAs significantly inhibited glucose-dependent increases in 30:0-, 32:0-, and 34:0-PA and moderately attenuated 30:1-, 32:1-, and 34:1-PA. Moreover, overexpression of DGKδ2 also enhanced the production of these PA species. MS/MS analysis revealed that these PA species commonly contain palmitic acid (16:0). D609, an inhibitor of phosphatidylcholine-specific phospholipase C (PC-PLC), significantly inhibited the glucose-stimulated production of the palmitic acid-containing PA species. Moreover, PC-PLC was co-immunoprecipitated with DGKδ2. These results strongly suggest that DGKδ preferably metabolizes palmitic acid-containing DG species supplied from the PC-PLC pathway, but not arachidonic acid (20:4)-containing DG species derived from the phosphatidylinositol turnover, in response to high glucose levels.

Type 2 diabetes is expected to afflict over 300 million people worldwide by 2015 (1). The characteristic features of type 2 diabetes include insulin resistance, glucose intolerance, hyperglycemia, and often, hyperinsulinemia (2). Glucose-induced insulin resistance is associated with a temporal increase in the intracellular diacylglycerol (DG)[2] mass in skeletal muscle (3).

DG is metabolized, at least in part, by DG kinase (DGK), which phosphorylates DG to generate phosphatidic acid (PA) (4–8). To date, 10 mammalian DGK isozymes (α, β, γ, δ, η, κ, ϵ, ζ, ι, and θ) have been identified, and these isozymes are subdivided into five groups according to their structural features (6, 7). Type II DGKs consist of the δ, η, and κ isoforms (9, 10). Moreover, alternatively spliced forms of DGKδ (δ1 and δ2) (11) and η (η1 and η2) (12) have been found.

DGKδ is highly expressed in skeletal muscle (13), which is a major insulin-target organ for glucose disposal (14). Chibalin *et al.* (15) demonstrated that DGKδ regulates glucose uptake and that a decrease in DGKδ expression resulted in the aggravation of type 2 diabetes. Long term exposure (96 h) to high glucose medium decreased DGKδ protein levels in primary cultured skeletal muscle cells, and the transcription of DGKδ and the levels of DGKδ protein were also reduced in skeletal muscles from type 2 diabetes patients (15). Moreover, DGKδ haploinsufficient mice (DGKδ$^{+/-}$) exhibited decreased total DGK activity, reduced DGKδ protein levels, and the accumulation of DG in skeletal muscle. The increase in the amount of DG caused the increase in the phosphorylation of protein kinase C (PKC) δ and a reduction in the expression of the insulin receptor and insulin receptor substrate-1 proteins involved in insulin signaling (15). Furthermore, Miele *et al.* (16) reported that acute high glucose exposure (within 5 min) increased DGKδ activity in skeletal muscle cells followed by a reduction of PKCα activity and transactivation of the insulin receptor signal.

* This work was supported in part by grants from the Ministry of Education, Culture, Sports, Science and Technology of Japan; the Japan Science and Technology Agency; the Naito Foundation; the Hamaguchi Foundation for the Advancement of Biochemistry; the Daiichi-Sankyo Foundation of Life Science; the Terumo Life Science Foundation; the Futaba Electronic Memorial Foundation; the Daiwa Securities Health Foundation; the Ono Medical Research Foundation; the Japan Foundation for Applied Enzymology; and the Food Science Institute Foundation.
[1] To whom correspondence should be addressed. Tel./Fax: 81-43-290-3695; E-mail: sakane@faculty.chiba-u.jp.

[2] The abbreviations used are: DG, diacylglycerol; DGK, DG kinase; D609, *O*-tricyclo[5.2.1.0^{2,6}]dec-9-yl dithiocarbonate; FIPI, 5-fluoro-2-indolyl deschlorohalopemide; ESI, electrospray ionization; PA, phosphatidic acid; PC, phosphatidylcholine; PC-PLC, PC-specific phospholipase C; PLD, phospholipase D; TOFA, 5-(tetradecyloxy)-2-furoic acid; PI, phosphatidylinositol; DMSO, dimethyl sulfoxide; AcGFP, GFP from *Aequorea coerulescens*.

Hence, these studies indicate that DG consumed by DGKδ in response to high glucose exposure is a key regulator of glucose uptake in skeletal muscle cells. DGKδ1 translocated from the cytoplasm to the plasma membrane in mouse myoblast C2C12 cells within 5 min of short term exposure to a high glucose concentration, whereas DGKδ2 was located in punctate vesicles irrespective of the glucose concentration (17).

Mammalian cells contain at least 50 structurally distinct molecular DG species because DG contains a variety of fatty acyl moieties at positions 1 and 2 (18). In general, DGs containing arachidonic acid (20:4), especially 18:0/20:4-DG (38:4-DG), in the phosphatidylinositol (PI) turnover are important molecules that serve as second messengers for PKC activation (18). Moreover, previous studies have demonstrated that DGKε preferably phosphorylates arachidonic acid-containing DGs derived from PI turnover (19, 20). Therefore, it is generally believed that all DGKs preferentially metabolize 38:4-DG for the regulation of signal transduction. However, the DG molecular species phosphorylated by DGKδ in response to glucose stimulation remain unknown.

In this study, we investigated the changes in the amounts of PA molecular species that are produced by DGK in glucose-stimulated C2C12 myoblasts using our previously developed liquid chromatography/electrospray ionization mass spectrometry (LC/ESI-MS) method (21) to identify the DG molecular species metabolized by DGKδ under short term high glucose conditions. Interestingly, the LC/ESI-MS analyses indicated that DGKδ preferably metabolizes limited DG molecular species, 30:0-, 30:1-, 32:0-, 32:1-, 34:0-, and 34:1-DG, commonly containing palmitic acid (16:0), but not DG species containing arachidonic acid in response to high glucose stimulation. Moreover, the 30:0-, 32:0-, and 34:0-DG species were suggested to be supplied by phospholipase C (PLC)-dependent phosphatidylcholine (PC) hydrolysis, indicating an unexpected linkage between PC-PLC and DGKδ.

EXPERIMENTAL PROCEDURES

Cell Culture—C2C12 mouse myoblasts were maintained on 100-mm dishes in DMEM (Wako Pure Chemicals) containing 10% FBS (Biological Industries-Invitrogen) at 37 °C in an atmosphere containing 5% CO_2. For differentiation to myotubes, confluent C2C12 myoblasts were cultured in differentiation medium (DMEM containing 0.1% FBS and 5 μg/ml insulin (Sigma-Aldrich)) for 4 days.

Establishment of a Stable Cell Line Overexpressing DGKδ—To establish C2C12 cells stably expressing human DGKδ2, the cells were transfected with pAcGFP-DGKδ2 (11, 17) using PolyFect (Qiagen) according to the instruction manual and were selected with 800 μg/ml G418 for 2 weeks. Single colonies were isolated and then were then grown in DMEM containing 10% FBS.

RNA Interference—To silence the expression of mouse DGKδ, the following Stealth RNAi duplexes (Invitrogen) were used: DGKδ-siRNA-1, 5′-GAAUGUGAUGCUGGAUCUUACUAAA-3′ and 5′-UUUAGUAAGAUCCAGCAUCACAUUC-3′; DGKδ-siRNA-2, 5′-UGGCAUUGGCUUGGAUGCAAAGAUA-3′ and 5′-UAUCUUUGCAUCCAAGCCAAUGCCA-3′. The duplexes were transfected into C2C12 myoblasts by electroporation (at 350 V and 300 microfarads) using the Gene Pulser Xcell™ electroporation system (Bio-Rad Laboratories). The transfected cells were then allowed to grow for 48 h in DMEM containing 10% FBS.

Glucose Stimulation and Treatment with Lipid Metabolism Enzyme Inhibitors—Glucose stimulation was performed as reported previously (16). Briefly, untransfected C2C12 myoblasts and C2C12 myoblasts transfected with Stealth RNAi duplexes were grown on poly-L-lysine (Sigma-Aldrich)-coated culture dishes. The cells were rinsed and incubated in glucose-free medium (16) in the absence or presence of PC-PLC inhibitor *O*-tricyclo[5.2.1.$0^{2,6}$]dec-9-yl dithiocarbonate (D609, 100 μM, Calbiochem) (22), acetyl-CoA carboxylase inhibitor 5-(tetradecyloxy)-2-furoic acid (TOFA, 20 μM, Calbiochem) (23, 24), or phospholipase D (PLD) inhibitor 5-fluoro-2-indolyl deschlorohalopemide (FIPI, 100 nM, Calbiochem) (25) for 3 h. The cells were incubated for 5 min in the same buffer supplemented with 25 mM glucose.

Lipid Extraction and Western Blot Analysis—The cells grown under each culture condition were harvested and lysed in ice-cold lysis buffer (50 mM HEPES, pH 7.2, 150 mM NaCl, 5 mM $MgCl_2$, 1 mM dithiothreitol, cOmplete™ EDTA-free protease inhibitor (Roche Diagnostics)) followed by centrifugation at 1,000 × *g* for 5 min at 4 °C. Total lipids were extracted from the cell lysates (1.0 mg of protein), in which DGKδ expression was confirmed by Western blot analysis using an anti-DGKδ antibody (13), according to the method of Bligh and Dyer (26). The extracted lipids were used for subsequent MS analyses.

Analysis of PA Molecular Species—PAs in extracted cellular lipids (5 μl) containing 40 pmol of the 14:0/14:0-PA internal standard (Sigma-Aldrich) were analyzed separately by LC/ESI-MS using an Accela LC system (Thermo Fisher Scientific) coupled online to an Exactive Orbitrap MS (Thermo Fisher Scientific) equipped with an ESI source as described previously (21). The MS peaks are presented in the form of *X*:*Y*, where *X* is the total number of carbon atoms and *Y* is the total number of double bonds in both acyl chains of the PA.

For the identification of fatty acid residues in PA molecular species by ESI-MS/MS, PA molecular species (28:0–40:0-PA) were fractionated using the above LC/ESI-MS system equipped with an FC 203B fraction collector (Gilson). The mixture of these isolated PA molecular species was infused into an Exactive Orbitrap MS (Thermo Fisher Scientific) equipped with a syringe pump (an infusion rate of 5 μl/min) and an ESI source. A collision energy of 40 eV was used to obtain fragment ions.

Analysis of DG Molecular Species—The isolation of DG was performed according to previously reported procedures (27). The extracted cellular lipids (per 1 mg of protein) were developed on Silica Gel 60 high performance thin layer chromatography plates (Merck, 10 × 20 cm) using hexane/diethyl ether/acetic acid (75:25:1, v/v). After development, DG was extracted from silica gel and redissolved in 200 μl of methanol:chloroform (9:1, v/v) containing 1 μg/ml 12:0/12:0-DG (Avanti Polar Lipids), and 10 μl of 100 mM sodium acetate were added to each sample (28). MS analysis was performed on an Exactive Orbitrap MS (Thermo Fisher Scientific) equipped with a Fusion 100T syringe pump (an infusion rate of 5 μl/min, Thermo Fisher Scientific) and an ESI source. The ion spray

voltage was set to 5 kV in the positive ion mode. The capillary temperature was set to 300 °C.

Measurement of DGKδ Activity—The octyl glucoside-mixed micellar assay of DGK activity was performed as described previously (12). COS-7 cells transfected with p3×FLAG-DGKδ2 (29) were harvested and lysed in ice-cold lysis buffer followed by centrifugation at 1,000 × *g* for 5 min at 4 °C. The cell lysates were added to octyl glucoside buffer containing 2 mM 16:0/16:0-, 16:0/18:1-, or 18:0/20:4-DG (Avanti Polar Lipids) and 10 mM phosphatidylserine (Avanti Polar Lipids).

Immunoprecipitation and Measurement of PC-PLC Activity—The glucose-stimulated cells stably expressing human DGKδ2 were harvested and lysed in ice-cold lysis buffer (50 mM HEPES, pH7.2, 150 mM NaCl, 5 mM $MgCl_2$, 1% Nonidet P-40, 1 mM dithiothreitol, cOmplete™ EDTA-free protease inhibitor (Roche Diagnostics)) for immunoprecipitation. The mixtures were centrifuged at 12,000 × *g* for 5 min at 4 °C to yield the cell lysates. 500 μg of the cell lysates were incubated with normal rabbit IgG (2 μg, Santa Cruz Biotechnology) or rabbit anti-DGKδ antibody (2 μg) (13, 29) at 4 °C overnight and incubated with protein A/G PLUS-agarose (Santa Cruz Biotechnology) for an additional 1 h. The bead-bound proteins were washed with ice-cold wash buffer (50 mM HEPES, pH 7.2, 100 mM NaCl, 5 mM $MgCl_2$, 0.1% Triton X-100, 10% glycerol, 20 mM NaF) four times and resolved in 70 μl of 1× reaction buffer (50 mM Tris-HCl, pH 7.4, 140 mM NaCl, 10 mM dimethylglutarate, 2 mM $CaCl_2$) in the Amplex Red® PC-PLC assay kit (Molecular Probes-Life Technologies). In this enzyme-coupled assay, PC-PLC activity is monitored indirectly using 10-acetyl-3,7-dihydroxyphenoxazine (Amplex Red® reagent), a sensitive fluorogenic probe for H_2O_2. First, PC-PLC converts PC to form phosphocholine and DG. After the action of alkaline phosphatase, which hydrolyzes phosphocholine, choline is oxidized by choline oxidase to betaine and H_2O_2. Finally, H_2O_2, in the presence of horseradish peroxidase, reacts with Amplex Red® reagent in a 1:1 stoichiometry to generate the highly fluorescent product, resorufin. Resorufin has absorption and fluorescence emission maxima of ~571 nm and 585 nm, respectively. 50-μl aliquots of the mixtures were used for the measurement of PC-PLC activities, and 10 μl of the mixtures were used for Western blot analysis.

Statistics—All LC/ESI-MS data were normalized based on the protein content and the intensity of the internal standard. The data were represented as the mean ± S.D. Statistical analysis was performed using the two-tailed *t* test or analysis of variance followed by Tukey's post hoc test.

RESULTS

Increase in the Amount of PA by Acute Stimulation with High Glucose—We first examined whether the amount of total PA was increased in C2C12 myoblasts stimulated with 25 mM glucose. As shown in Fig. 1*A*, LC/ESI-MS analysis indicated that exposure to high glucose levels (for 5 min) statistically increased the total PA amounts (1.23-fold, $p < 0.005$). In addition, the stimulation significantly increased the amounts of C30 to C36 PA molecular species, with the exception of 36:1-PA (Fig. 1*B*). However, the stimulation did not substantially affect the production of C38 to C40 PA molecular species, including 38:4-PA, with the exception of 38:6-PA.

We investigated the high glucose-dependent increases of total PA amount and PA molecular species in C2C12 myoblasts at different time points. After 5 min of glucose stimulation, the levels of total PA and PA molecular species were significantly increased (Fig. 1, *C* and *D*). However, total PA and PA molecular species levels returned close to basal levels by prolonging the incubation with high glucose concentrations for up to 15 and 30 min. We confirmed that DGK activity *in vitro* was increased by glucose stimulation for 5 min (data not shown). These results strongly suggest that C2C12 myoblasts and L6 myotubes (16) have essentially the same lipid metabolism pathway to produce PA in response to acute glucose stimulation.

We confirmed the changes in the amounts of PA molecular species in C2C12 myotubes in response to acute high glucose stimulation (5 min). The glucose-stimulated C2C12 myotubes showed essentially the same results (Fig. 1, *E* and *F*) as those obtained with C2C12 myoblasts (Fig. 1, *A* and *B*). The results support that C2C12 myoblasts and myotubes possess essentially the same lipid metabolism pathway to produce PA in response to high glucose stimulation. Because C2C12 myoblasts were more efficiently transfected with siRNAs than C2C12 myotubes, C2C12 myoblasts were used for identification of PA molecular species produced by DGKδ in response to high glucose stimulation.

Effects of DGKδ-specific siRNAs on High Glucose-induced Increases in PA Molecular Species—To clarify whether the glucose-stimulated production of PA molecular species is catalyzed by DGKδ, we investigated the effects of a DGKδ-specific siRNA, DGKδ-siRNA-1. Of the two alternatively spliced DGKδ products, DGKδ1 and DGKδ2 (11), C2C12 myoblasts predominantly expressed DGKδ2 (Fig. 2*A*). DGKδ-siRNA-1 efficiently suppressed DGKδ2 expression in C2C12 myoblasts (Fig. 2*A*). To facilitate comparison, averages of the relative values (+glucose *versus* −glucose) from four independent experiments are displayed (Fig. 2*B*). Interestingly, the suppression of DGKδ expression by DGKδ-siRNA-1 significantly inhibited the glucose stimulation-dependent production of saturated fatty acid-containing C30-C34 PA species, 30:0-, 32:0-, and 34:0-PA, to their basal levels. In addition, one saturated and one monounsaturated fatty acid-containing PA, 34:1-PA, decreased as well. However, the amount of arachidonic acid (20:4)-containing PA, 38:4-PA, was not markedly changed (Fig. 2*B*). To rule out off-target effects of DGKδ-siRNA-1, we employed an independent siRNA targeted to a different region of DGKδ mRNA (DGKδ-siRNA-2). DGKδ-siRNA-2, which suppressed DGKδ2 expression slightly less strongly than DGKδ-siRNA-1 (Fig. 2*C*), also statistically inhibited the production of 30:0-, 34:1-, and 34:0-PA and moderately attenuated 32:0-PA generation (Fig. 2*D*). These results suggest that DGKδ selectively phosphorylated 30:0-, 32:0-, 34:1-, and 34:0-DG, which contain either two saturated fatty acids or one saturated and one monounsaturated fatty acids, but not 38:4-PA.

We investigated whether the decreases in the amounts of 30:0-, 32:0-, 34:1-, and 34:0-PA by DGKδ-siRNAs were due to decreases in the substrates, the corresponding DG species, in high glucose-stimulated and -unstimulated C2C12 myoblasts.

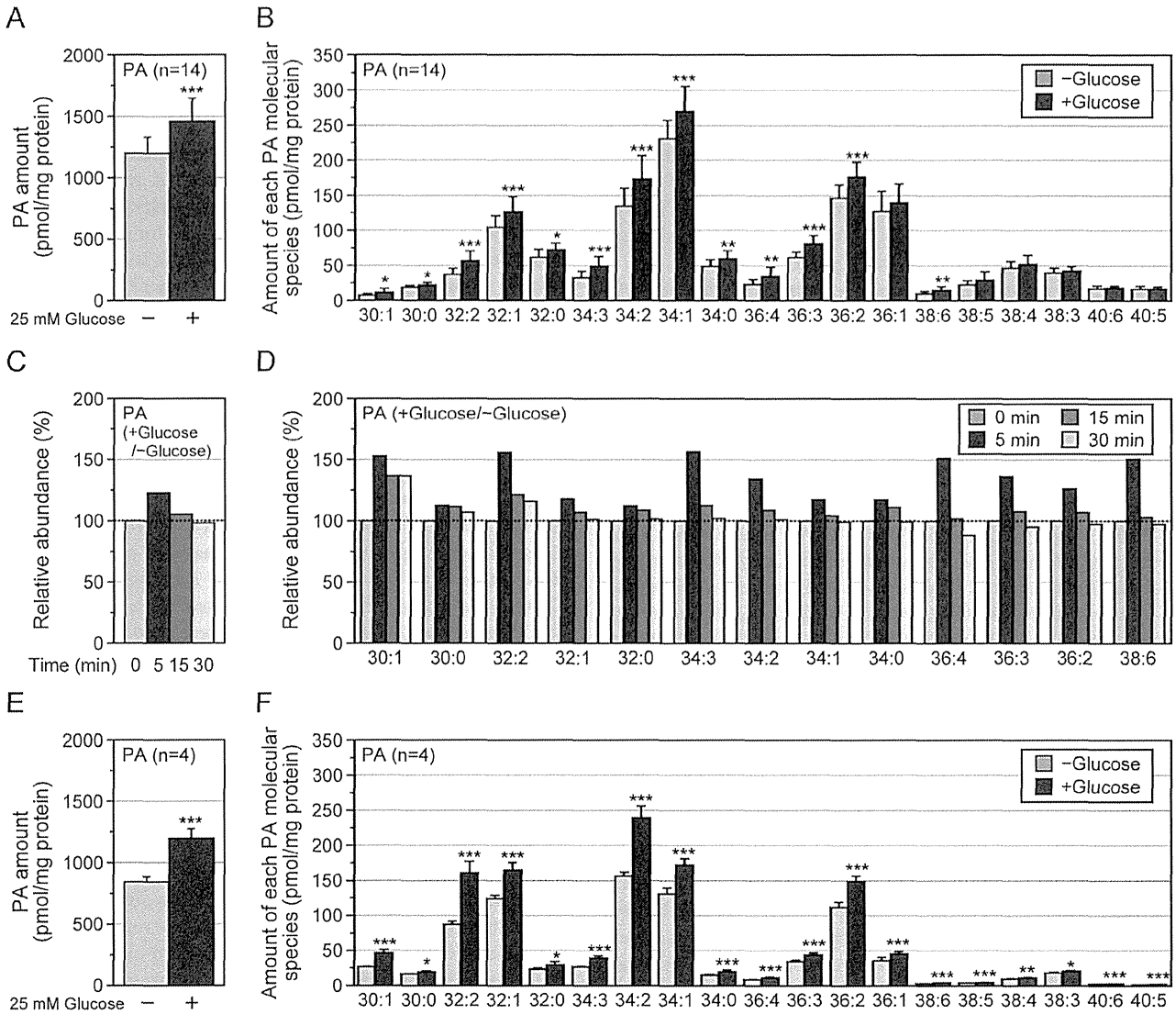

FIGURE 1. **Changes in the total PA and PA molecular species by high glucose stimulation in C2C12 myoblasts and myotubes.** *A* and *B*, the amounts of the total PAs (*A*) and major PA molecular species (*B*) in the glucose-unstimulated or glucose-stimulated C2C12 myoblasts were quantified using the LC/ESI-MS method. The values are presented as the mean ± S.D. ($n = 14$). *, $p < 0.05$; **, $p < 0.01$; ***, $p < 0.005$ (no stimulation *versus* glucose stimulation). *C* and *D*, the amounts of the total PAs (*C*) and major PA molecular species (*D*) that statistically increased in *A* in the cells stimulated by glucose for 5, 15, or 30 min were detected using the LC/ESI-MS method. The results are presented as the percentage of the value of PA molecular species in glucose-unstimulated cells. The values are presented as the mean ($n = 2$). Essentially the same results were obtained in two independent experiments. *E* and *F*, the amounts of the total PAs (*E*) and major PA molecular species (*F*) in the glucose-unstimulated or glucose-stimulated C2C12 myotubes were quantified using the LC/ESI-MS method. The values are presented as the mean ± S.D. ($n = 4$). *, $p < 0.05$; **, $p < 0.01$; ***, $p < 0.005$ (no stimulation *versus* glucose stimulation).

Glucose stimulation substantially increased the amounts of various DG species (Fig. 3). However, DGKδ-siRNA-1 failed to significantly affect the amounts of 30:0-, 32:0-, 34:1-, and 34:0-DG molecular species both in the absence and in the presence of high glucose levels. Therefore, it is likely that the decreases in the amounts of 30:0-, 32:0-, 34:1-, and 34:0-PA were not caused by decreased amounts of the corresponding DG species.

Effect of Overexpression of DGKδ on the Production of PA Molecular Species—To confirm the results of the siRNA experiments, we evaluated the result of DGKδ2 overexpression on high glucose-dependent production of PA species in C2C12 cells. In response to high glucose, the levels of 30:0-, 32:0-, and 34:0-PA statistically increased in C2C12 cells stably expressing DGKδ2 when compared with control cells (Fig. 4*B*). Moreover, 30:1- and 32:1-PA were also augmented. In contrast, 38:4-PA did not increase. Taken together with the siRNA results (Figs. 2 and 4), these results support the hypothesis that DGKδ phosphorylated DG species with an apparent preference for 30:0-, 32:0-, and 34:0-DG, but not arachidonic acid-containing DG, 38:4-DG. Moreover, it is possible that this enzyme also generates 30:1-, 32:1-, and 34:1-PA.

Fatty Acid Composition of 30:0-, 32:0-, and 34:0-PA—We next determined the molecular identities of the two fatty acids included in 30:0-, 32:0-, and 34:0-PA, which were indicated to be selectively generated by DGKδ2 in C2C12 cells. ESI-MS/MS

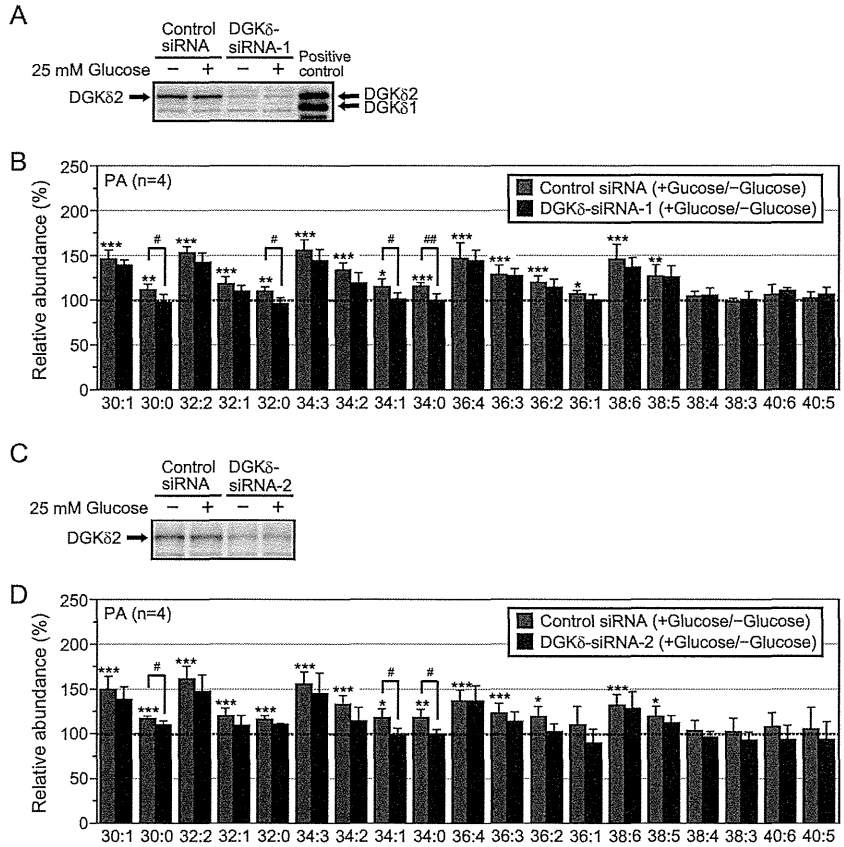

FIGURE 2. **Effects of DGKδ-siRNA-1 and -2 on high glucose-induced increases of PA molecular species in C2C12 myoblasts.** *A* and *C*, the suppression of DGKδ2 expression by DGKδ-siRNA-1 (*A*) or DGKδ-siRNA-2 (*C*) was confirmed by Western blot analysis using the anti-DGKδ antibody. Human DGKδ1 and DGKδ2 (11) expressed in COS-7 cells were electrophoresed as a control (*A*). *B* and *D*, the major PA molecular species in the glucose-unstimulated or glucose-stimulated cells transfected with control siRNA or DGKδ-siRNA-1/2 were detected using the LC/ESI-MS method. The results are presented as the percentage of the value of PA molecular species in glucose-unstimulated cells transfected with control siRNA or DGKδ-siRNA-1/2. DGKδ-siRNA-1/2 did not significantly affect the value of PA molecular species in glucose-unstimulated cells. The values are presented as the mean ± S.D. ($n = 4$). *, $p < 0.05$; **, $p < 0.01$; ***, $p < 0.005$ (no stimulation *versus* glucose stimulation). #, $p < 0.05$; ##, $p < 0.01$ (control siRNA *versus* DGKδ-siRNA-1 or DGKδ-siRNA-2).

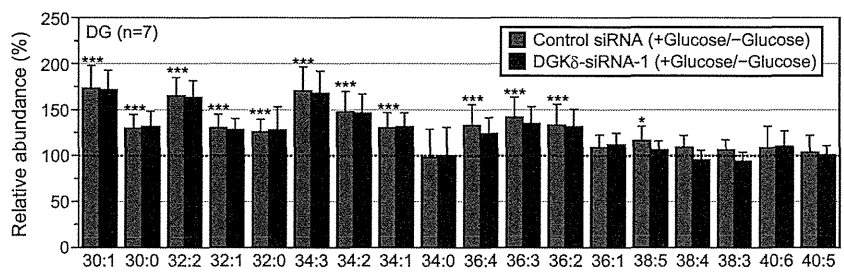

FIGURE 3. **Effect of DGKδ-siRNA-1 on high glucose-induced increases of DG molecular species in C2C12 myoblasts.** The major DG molecular species in the glucose-unstimulated or glucose-stimulated cells transfected with control siRNA or DGKδ-siRNA-1 were detected using the ESI-MS method. The results are presented as the percentage of the value of DG molecular species in glucose-unstimulated cells transfected with control siRNA or DGKδ-siRNA-1. DGKδ-siRNA-1 did not significantly affect the value of DG molecular species in glucose-unstimulated cells. The values are presented as the mean ± S.D. ($n = 7$). *, $p < 0.05$; ***, $p < 0.005$ (no stimulation *versus* glucose stimulation).

analysis revealed that the main fatty acid residues were as follows: 30:0 consisted of 14:0 and 16:0 (100%), 32:0 included 16:0 and 16:0 (96.6%), and 34:0 contained 16:0 and 18:0 (99.7%) (Table 1). These results indicate that 30:0-, 32:0-, and 34:0-PA consist of relatively short saturated fatty acids and commonly contain palmitic acid (16:0). It is possible that DGKδ2 also produces 30:1-, 32:1-, and 34:1-PA species (Figs. 2 and 4). These PA species contain saturated fatty acids, 16:0 and 14:0, and monounsaturated fatty acids, 16:1 and 18:1 (Table 1).

In Vitro DGKδ Activity—We examined whether the preference of DGKδ2 for palmitic acid (16:0)-containing DG species, 30:0-, 32:0-, and 34:0-DG, is an intrinsic catalytic feature of DGKδ. To this end, we measured DGKδ2 activity *in vitro* using 32:0 (16:0/16:0)-, 34:1 (16:0/18:1)-, or 38:4 (18:0/20:4)-DG as

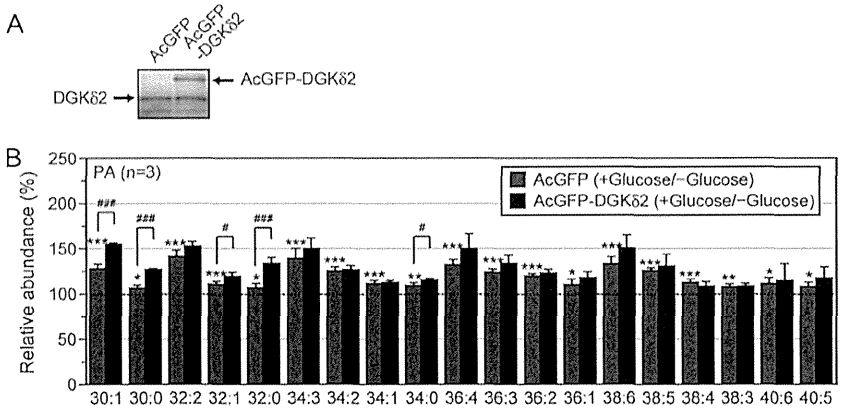

FIGURE 4. **PA molecular species in C2C12 cells stably expressing DGKδ2.** *A*, the stable expression of AcGFP-DGKδ2 in C2C12 cells was confirmed by Western blot analysis using the anti-DGKδ antibody. *B*, the major PA molecular species in the glucose-unstimulated or glucose-stimulated cells stably expressing human DGKδ2 were identified and quantified using LC/ESI-MS. The results are presented as the percentage of the value of PA molecular species in glucose-unstimulated cells transfected with AcGFP alone or AcGFP-DGKδ2. Overexpression of DGKδ2 did not significantly affect the value of PA molecular species in glucose-unstimulated cells. The values are presented as the mean ± S.D. ($n = 3$). *, $p < 0.05$; **, $p < 0.01$; ***, $p < 0.005$ (no stimulation *versus* glucose stimulation). #, $p < 0.05$; ###, $p < 0.005$ (no overexpression *versus* DGKδ overexpression).

TABLE 1

Identification of the acyl species in each PA molecular species

PA molecular species	Identified acyl chains[a]			
	%			
30:1	14:0/16:1 (86.0%)	16:0/14:1 (14.0%)		
30:0	14:0/16:0 (100%)			
32:2	16:1/16:1 (98.5%)	14:0/18:2 (1.5%)		
32:1	16:0/16:1 (88.7%)	14:0/18:1 (11.3%)		
32:0	16:0/16:0 (96.6%)	14:0/18:0 (3.4%)		
34:3	16:1/18:2 (67.2%)	16:2/18:1 (27.7%)	16:0/18:3 (5.1%)	
34:2	16:1/18:1 (86.3%)	16:0/18:2 (13.6%)	16:2/18:0 (0.1%)	
34:1	16:0/18:1 (93.2%)	18:0/16:1 (6.8%)		
34:0	16:0/18:0 (99.7%)	14:0/20:0 (0.3%)		
36:4	16:0/20:4 (83.0%)	16:1/20:3 (8.7%)	18:1/18:3 (7.2%)	18:2/18:2 (1.2%)
36:3	18:1/18:2 (74.9%)	16:0/20:3 (23.6%)	16:1/20:2 (0.8%)	18:0/18:3 (0.7%)
36:2	18:1/18:1 (91.6%)	18:0/18:2 (5.0%)	16:0/20:2 (2.5%)	16:1/20:1 (0.9%)
36:1	18:0/18:1 (87.8%)	16:0/20:1 (6.5%)	16:1/20:0 (5.6%)	14:0/22:1 (0.1%)
38:6	16:0/22:6 (68.0%)	16:1/22:5 (30.9%)	18:1/20:5 (1.1%)	
38:5	16:0/22:5 (45.0%)	18:1/20:4 (45.0%)	18:0/20:5 (8.5%)	16:1/22:4 (1.6%)
38:4	18:0/20:4 (80.1%)	18:1/20:3 (19.5%)	16:0/22:4 (0.4%)	
38:3	18:0/20:3 (88.6%)	18:1/20:2 (10.5%)	16:0/22:3 (0.9%)	
40:6	18:1/22:5 (51.5%)	18:0/22:6 (47.6%)	16:0/24:6 (0.9%)	
40:5	18:0/22:5 (97.4%)	18:1/22:4 (2.6%)		

[a] The relative abundance (%) was based on the peak areas of the fragment ions (ESI-MS/MS) for each molecular ion.

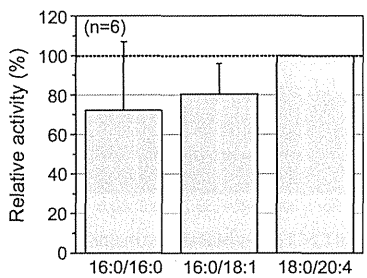

FIGURE 5. ***In vitro* DGKδ activity.** For measurement of *in vitro* DGKδ activity, 2 mM (5.4 mol%) 16:0/16:0-, 16:0/18:1-, and 18:0/20:4-DG were used as substrates. The activity of 3×FLAG-tagged DGKδ2 in COS-7 cells was compared with the control. The results are presented as the percentage of the value of activity against 18:0/20:4-DG. The values are presented as the mean ± S.D. ($n = 6$).

substrates. As shown in Fig. 5, the levels of 32:0- and 34:1-PA generated by DGKδ2 were similar to or slightly lower than that of 38:4-PA. These results indicate that DGKδ2 does not exhibit intrinsic substrate selectivity for particular DG molecular species, 32:0-DG, *in vitro*. Therefore, we hypothesized that DGKδ accomplishes apparent substrate selectivity in C2C12 cells by accessing a DG pool containing only 30:0-, 32:0-, and 34:0-DG, and not based on the intrinsic properties of the enzyme.

Effects of Inhibitors of Lipid Metabolism Enzymes on High Glucose Level-induced PA Production—To test this hypothesis, we next searched for the lipid metabolic pathway that supplies 30:0-, 32:0-, and 34:0-DG species as a substrate for DGKδ2. There are three pathways that produce DG, 1) the *de novo* pathway (30, 31), 2) the PLD/PA phosphatase pathway (32), and 3) the PC-specific PLC pathway (33). The treatment with 20 μM TOFA, which inhibits acetyl-CoA carboxylase involved in the *de novo* synthesis of DG (23, 24), did not decrease the glucose-stimulated production of PA molecular species (Fig. 6*A*). Moreover, 100 nM FIPI, which inhibits PLD involved in DG generation from PC through the action of PA phosphatase (25), reduced the amounts of most of the PAs in the absence of high glucose stimulation (data not shown). However, this compound failed to attenuate the glucose-stimulated production of PA molecular species (Fig. 6*B*). These results strongly suggest that these pathways are not involved in the DG supply to DGKδ2.

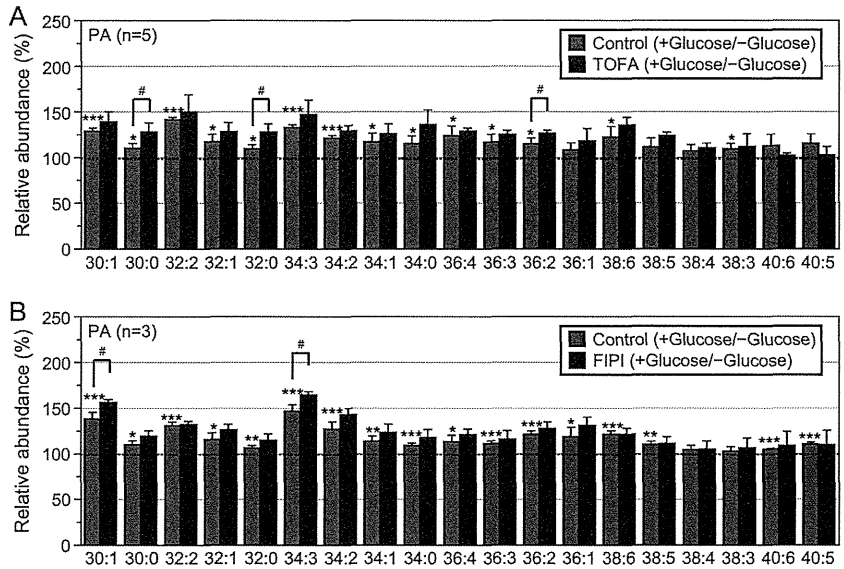

FIGURE 6. **Effects of TOFA and FIPI on the production of PA molecular species in glucose-stimulated C2C12 cells.** *A*, the major PA molecular species in glucose-unstimulated or glucose-stimulated cells treated with DMSO (control) or TOFA were detected using the LC/ESI-MS method. The results are presented as the percentage of the value of PA species in glucose-unstimulated cells treated with DMSO (control) or TOFA. The values are presented as the mean ± S.D. ($n = 5$). *, $p < 0.05$; ***, $p < 0.005$ (no stimulation *versus* glucose stimulation). #, $p < 0.05$ (without TOFA *versus* with TOFA). *B*, the major PA molecular species in the glucose-unstimulated or glucose-stimulated cells treated with DMSO (control) or FIPI were detected using the LC/ESI-MS method. The results are presented as the percentage of the value of PA species in glucose-unstimulated cells treated with DMSO (control) or FIPI. The values are presented as the mean ± S.D. ($n = 3$). *, $p < 0.05$; **, $p < 0.01$; ***, $p < 0.005$ (no stimulation *versus* glucose stimulation). #, $p < 0.05$ (without FIPI *versus* with FIPI).

D609 is an inhibitor of PC-PLC (22), which generates DG via PC hydrolysis (34). Treatment with 100 μM D609 strongly inhibited the high glucose stimulation-responsive production of 30:0-, 32:0-, and 34:0-PA to their basal levels (Fig. 7*A*), suggesting that DGKδ2 utilizes DG species supplied from the PC-PLC pathway.

We next confirmed that D609 inhibited the production of DG molecular species, including 30:0-, 32:0-, and 34:0-DG. This inhibitor statistically attenuated the amounts of 30:0-, 32:0-, and 34:0-DG in the absence of high glucose stimulation (Fig. 7*B*). However, D609 inhibited high glucose-dependent increases for all of the C30-C34 DG species (Fig. 7*C*). These results suggest that, in response to acute high glucose stimulation (5 min), DGKδ2 can utilize DG species that are supplied from the PC-PLC pathway, in both high glucose-independent and high glucose-dependent manners.

Linkage between PC-PLC and DGKδ—To further examine the linkage between the PC-PLC pathway and DGKδ2, we determined whether D609 and DGKδ-siRNA-1 additively affected the high glucose-dependent increases of 30:0-, 32:0-, and 34:0-PA. If DGKδ2 utilizes DG species supplied from the PC-PLC pathway, it would be expected that reduced expression of DGKδ2 via DGKδ-siRNA-1 would not enhance the effect of the PC-PLC inhibitor. It was confirmed that the expression of DGKδ2 was substantially reduced by DGKδ-siRNA-1, even in the presence of D609 (Fig. 8*A*). As shown in Fig. 8*B*, DGKδ-siRNA-1 failed to further inhibit the glucose-dependent increases of 30:0-, 32:0-, and 34:0-PA in the presence of D609. These results strongly suggest that 30:0-, 32:0-, and 34:0-DG phosphorylated by DGKδ2 in response to acute high glucose exposure are generated, at least in part, by PC hydrolysis catalyzed by PC-PLC.

We next examined whether DGKδ directly or indirectly interacted with PC-PLC. To this end, we used C2C12 cells stably overexpressing DGKδ2 (Fig. 4) and stimulated the cells with high glucose. We confirmed that DGKδ2 was immunoprecipitated with the anti-DGKδ antibody (Fig. 8*C*). Because the molecular identity of mammalian PC-PLC remains unclear (35), its antibody is unavailable. Therefore, we determined PC-PLC activity in the immunoprecipitates using the Amplex Red® PC-PLC assay kit, which detects phosphocholine generated by PC-PLC. As demonstrated in Fig. 8*D*, PC-PLC activity was clearly co-immunoprecipitated with DGKδ2. The assay does not detect the activity of sphingomyelin synthase, which produces DG and sphingomyelin, but not phosphocholine. The contribution of PLD, which hydrolyzes PC to PA and choline, can be accounted for by elimination of alkaline phosphatase from the assay (see "Experimental Procedures"). However, when the assay was performed in the absence of alkaline phosphatase, the activity was not detectable. Taken together, these results strongly suggest that DGKδ2 utilizes DG species supplied from PC-PLC-dependent PC hydrolysis in response to high glucose (Fig. 9).

DISCUSSION

The increase in PA molecular species by stimulation with high glucose levels has not been identified until now. Moreover, it has not been reported that high glucose induces total PA production. The main reasons for this are that PA species are minor components and it is difficult to quantify the amounts of PA molecular species using conventional LC/ESI-MS methods. To overcome this difficulty, we recently established an LC/ESI-MS method specialized for PA species (21). In this study, we revealed for the first time that acute high glucose

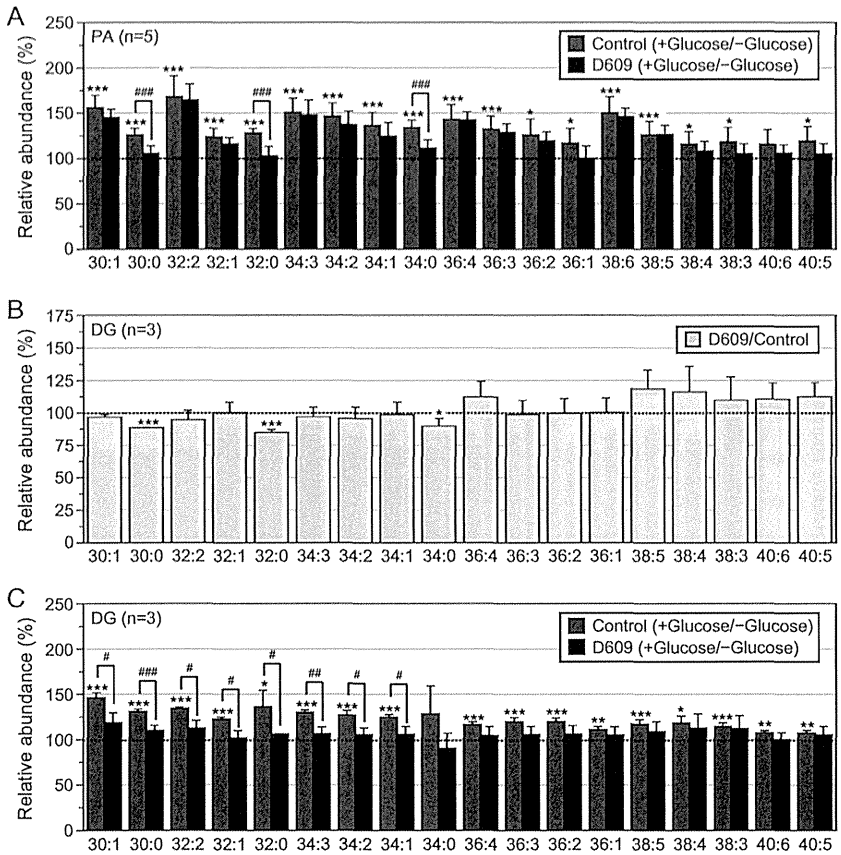

FIGURE 7. **Effect of D609 on high glucose-induced increases in PA and DG molecular species in C2C12 myoblasts.** *A*, the major PA molecular species in the glucose-unstimulated or glucose-stimulated cells treated with DMSO (control) or D609 were detected using the LC/ESI-MS method. The results are presented as the percentage of the value of PA molecular species in glucose-unstimulated cells treated with DMSO (control) or D609. D609 did not significantly affect the value of PA molecular species in glucose-unstimulated cells. The values are presented as the mean ± S.D. ($n = 5$). *, $p < 0.05$; ***, $p < 0.005$ (no stimulation *versus* glucose stimulation). ###, $p < 0.005$ (without D609 *versus* with D609). *B* and *C*, the major DG molecular species in the glucose-unstimulated or glucose-stimulated cells treated with DMSO (control) or D609 were detected using the ESI-MS method. *B*, comparison of +D609 *versus* −D609 in the absence of glucose. The results are presented as the percentage of the value of DG species in glucose-unstimulated cells treated with DMSO (control). The values are presented as the mean ± S.D. ($n = 3$). *, $p < 0.05$; ***, $p < 0.005$. *C*, comparison of +glucose *versus* −glucose in the absence or presence of D609. The results are presented as the percentage of the value of DG species in glucose-unstimulated cells treated with DMSO (control) or D609. D609 did not significantly affect the value of DG molecular species in glucose-unstimulated cells. The values are presented as the mean ± S.D. ($n = 3$). *, $p < 0.05$; **, $p < 0.01$; ***, $p < 0.005$ (no stimulation *versus* glucose stimulation). #, $p < 0.05$; ##, $p < 0.01$; ###, $p < 0.005$ (without D609 *versus* with D609).

stimulation statistically increased the PA mass and number of molecular species using the newly developed method (Fig. 1). The results indicate that our LC/ESI-MS method is a powerful tool for detecting even small changes in PA molecular species.

The suppression of DGKδ expression by RNA silencing decreased the high glucose-induced production of 30:0-, 32:0-, 34:1-, and 34:0-PA in C2C12 myoblasts (Fig. 2). Moreover, the levels of 30:1-, 30:0-, 32:1-, 32:0-, and 34:0-PA were substantially increased in a high glucose-dependent manner in C2C12 cells stably expressing DGKδ2 when compared with control cells (Fig. 4). Taken together, these results strongly suggest that DGKδ preferentially generates 30:0-, 32:0-, and 34:0-PA, which contain two saturated fatty acids, in the cells. The main fatty acid residues of these PA species were 14:0 and 16:0, 16:0 and 16:0, and 16:0 and 18:0, respectively (Table 1). These results suggest that DGKδ produces PA with an apparent preference for palmitic acid (16:0)-containing PA. Moreover, the suppression of DGKδ expression by siRNA-1 and -2 also decreased the high glucose-induced production of 34:1-PA (Fig. 2). The overexpression of DGKδ2 statistically increased the levels of 30:1- and 32:1-PA (Fig. 4). The DGKδ suppression also modestly attenuated 30:1- and 32:1-PA levels (Fig. 2), and the DGKδ2 overexpression slightly augmented 34:1-PA production (Fig. 4). Therefore, it is possible that this enzyme also generates 30:1-, 32:1-, and 34:1-PA, which contain one saturated and one monounsaturated fatty acid, in addition to 30:0-, 32:0-, and 34:0-PA. 30:1-, 32:1-, and 34:1-PA contain saturated fatty acids, 16:0 and 14:0, and monounsaturated fatty acids, 16:1 and 18:1 (Table 1). The DGKδ-siRNAs and DGKδ overexpression failed to statistically affect the amounts of high glucose-induced increases of 32:2-, 34:3-, 34:2-, 36:4-, 36:3-, 36:2-, and 38:6-PA (Figs. 2 and 4), implying that these PA species were generated by other DGK isozyme(s).

DGK is a member of the PI turnover pathway and initiates resynthesis of PI (18). This fact led us to believe that DGK isozymes, including DGKδ, also exhibit selectivity against 38:4 (18:0/20:4)-DG derived from PI turnover. Indeed, it was reported that DGKε preferentially phosphorylated DGs con-

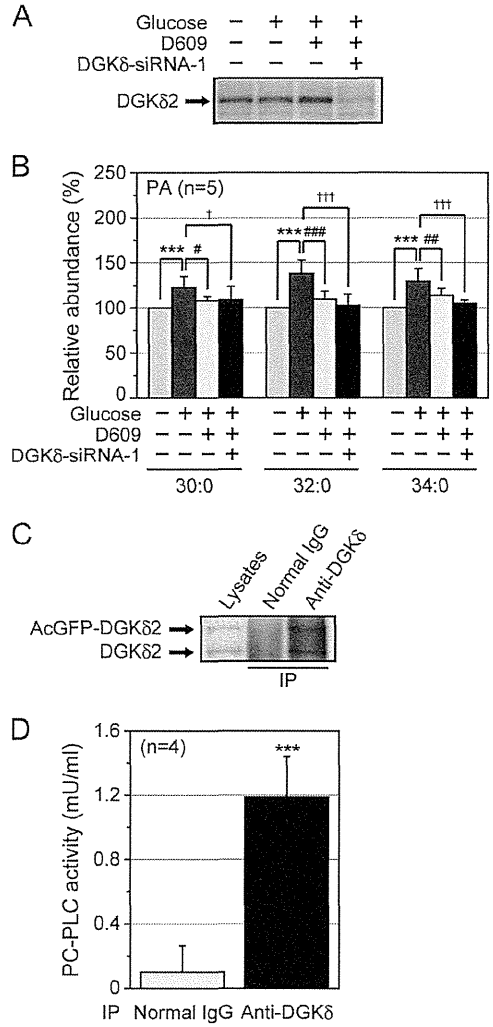

FIGURE 8. **Examination of the functional linkage between PC-PLC and DGKδ.** Effects of D609 and DGKδ-siRNA-1 on high glucose-induced increases of PA molecular species in C2C12 myoblasts were compared. *A*, the suppression of DGKδ2 expression by DGKδ-siRNA-1 was confirmed by Western blot analysis using the anti-DGKδ antibody. *B*, 30:0-, 32:0-, and 34:0-PA in the glucose-unstimulated or glucose-stimulated cells treated with DMSO (control), D609, or D609 and DGKδ-siRNA-1 were detected using the LC/ESI-MS method. The results are presented as the percentage of the value of PA molecular species in glucose-unstimulated cells. The values are presented as the mean ± S.D. ($n = 5$). ***, $p < 0.005$ (no stimulation *versus* glucose stimulation). #, $p < 0.05$; ##, $p < 0.01$; ###, $p < 0.005$ (without D609 *versus* with D609). †, $p < 0.05$; †††, $p < 0.005$ (control siRNA *versus* DGKδ-siRNA-1). *C* and *D*, co-immunoprecipitation of PC-PLC activity with DGKδ2. *C*, immunoprecipitation (*IP*) of DGKδ2 using the anti-DGKδ antibody was confirmed by Western blot analysis using the anti-DGKδ antibody. *D*, PC-PLC activity in the precipitates was measured using the Amplex Red® PC-PLC assay kit. The values are presented as the mean ± S.D. ($n = 4$). ***, $p < 0.005$. When the assay was performed in the absence of alkaline phosphatase, the activity was not detectable.

taining arachidonic acid (*e.g.* 38:4 (18:0/20:4)-DG) derived from PI turnover (7, 19, 20). However, high glucose stimulation did not increase the amount of 38:4-PA (Figs. 1 and 2), which mainly consisted of 18:0/20:4-PA (Table 1). Moreover, DGKδ-siRNAs and DGKδ2 overexpression failed to affect the amounts of 38:4-PA in response to high glucose stimulation (Figs. 2 and 4). These results indicate that DGKδ does not phosphorylate 38:4-DG derived from PI turnover in a glucose-dependent manner.

DGKδ did not exhibit selectivity against 16:0/16:0 (32:0)- or 16:0/18:1 (34:1)-DG *in vitro* (Fig. 5). Therefore, we hypothesized that DGKδ exerts substrate selectivity in C2C12 cells through accessing a DG pool containing 30:0-, 32:0-, and 34:0-DG, and not via its intrinsic preference. There are three DG supply pathways, *i.e.* 1) *de novo* synthesis including acetyl-CoA carboxylase (30, 31), 2) the PLD/PA phosphatase route (32), and 3) PC hydrolysis by PC-specific PLC (33). Treatment with the PC-PLC inhibitor D609, but not inhibitors of acetyl-CoA carboxylase and PLD, strongly inhibited the high glucose stimulation-responsive production of 30:0-, 32:0-, and 34:0-PA (Fig. 7*A*). Moreover, RNA silencing of DGKδ failed to further inhibit the glucose-dependent increases in 30:0-, 32:0-, and 34:0-PA in the presence of D609 (Fig. 8*B*). Furthermore, PC-PLC was co-immunoprecipitated with DGKδ2 (Fig. 8*D*). Taken together, these results strongly suggest that 30:0-, 32:0-, and 34:0-DG phosphorylated by DGKδ2 in response to acute high glucose exposure are generated, at least in part, by PC hydrolysis catalyzed by PC-PLC (Fig. 9).

The role of sphingomyelin synthase as a potential PC-PLC was indicated (36). We cannot rule out the possibility that DGKδ2 partly utilizes sphingomyelin synthase-dependent DG. However, it is likely that DGKδ2 phosphorylates DG species generated, at least in part, by PC-PLC because the co-immunoprecipitates with DGKδ2 contained PC-PLC activity.

The molecular identity of PC-PLC remains unclear (35). In this study, DGKδ was revealed to directly or indirectly associate with PC-PLC. With the pulldown of PC-PLC activity with DGKδ2, there may be an opportunity to identify the unidentified PC-PLC enzyme by proteomics approaches. Therefore, DGKδ2 may serve as a good tool to search for the PC-PLC molecule.

D609 attenuated high glucose-dependent increases in various C30-C34 DG species (Fig. 7*C*). However, D609 strongly inhibited only the high glucose stimulation-responsive production of 30:0-, 32:0-, and 34:0-PA (Fig. 7*A*). Intriguingly, this inhibitor statistically reduced the amounts of 30:0-, 32:0-, and 34:0-DG in the absence of high glucose (Fig. 7*B*). Therefore, it is likely that, in response to acute high glucose stimulation (5 min), DGKδ2 mainly utilizes these DG species supplied from the PC-PLC pathway in a high glucose-independent manner. Moreover, DGKδ2 can generate 30:1-, 32:1-, and 34:1-PA, in addition to 30:0-, 32:0-, and 34:0-PA. (Figs. 2 and 4). Although D609 moderately attenuated 30:1-, 32:1-, and 34:1-PA generation (Fig. 7*A*), this inhibitor did not affect the amounts of 30:1-, 32:1-, and 34:1-DG in the absence of high glucose stimulation (Fig. 7*B*). However, D609 substantially inhibited high glucose-dependent increases for 30:1-, 32:1-, and 34:1-DG (Fig. 7*C*). These results suggest that DGKδ2 can utilize 30:1-, 32:1-, and 34:1-DG that are supplied from the PC-PLC pathway in a high glucose-dependent manner.

Recently, Shulga *et al.* (37) and Lowe *et al.* (38) reported that DGKδ positively regulated lipid synthesis, including DG and PA, during adipocyte differentiation. However, unlike for acute high glucose stimulation, a significant preference against DG and PA was not found. The increases were, at least in part, a